sustainability

MDPI

Article

Shear Behavior of Geopolymer Concrete Beams Under Monotonic and Cyclic Loading

Musab Aied Qissab Al-Janabi [1,2], Duaa Al-Jeznawi [1], Rana Talib Nasser [1], Luís Filipe Almeida Bernardo [3,*], Ismacahyadi Bagus Mohamed Jais [4] and Hugo Alexandre Silva Pinto [3]

[1] Department of Civil Engineering, College of Engineering, Al-Nahrain University, Jadriya, Baghdad 10081, Iraq; musab.a.jindeel@nahrainuniv.edu.iq (M.A.Q.A.-J.); duaa.a.al-jeznawi@nahrainuniv.edu.iq (D.A.-J.); ranatnasser84@gmail.com (R.T.N.)
[2] Department of Civil Engineering, Middle East Technical University, Ankara 06800, Türkiye
[3] GeoBioTec, Department of Civil Engineering, University of Beira Interior, 6201-001 Covilhã, Portugal; hpinto@ubi.pt
[4] GeoForenSIG, Faculty of Civil Engineering, Universiti Teknologi MARA, Shah Alam 40450, Malaysia; ismac821@uitm.edu.my
* Correspondence: lfb@ubi.pt

Abstract

This study examines the shear behavior of geopolymer (zero-cement) concrete (ZCC) beams under monotonic and cyclic loading, focusing on the effects of concrete compressive strength, reinforcement ratio, and shear span-to-depth ratio. A total of 48 simply supported beams were tested under two-point loading, with compressive strengths of 20 and 30 MPa, longitudinal reinforcement configurations of 2Ø10, 3Ø10, and 3Ø12, and shear span-to-depth ratios (a/d) of 2, 2.5, and 3. The results demonstrate that ZCC beams achieve shear capacity, ductility, and energy dissipation comparable to or exceeding those of conventional concrete beams, confirming their suitability for shear-critical structural applications and providing valuable experimental data to support future design and modeling of sustainable concrete systems. Results showed that under monotonic loading, increasing compressive strength and longitudinal reinforcement enhanced load capacity by up to 33%, improved energy absorption, and reduced deflection, while higher a/d ratios decreased load capacity by about 37% but increased deflection by nearly 48%. Similar trends were observed under cyclic loading, although beams exhibited additional vertical cracking and stiffness degradation; ZCC beams sustained 70–90% of their monotonic displacement capacity, with 30 MPa specimens demonstrating superior energy dissipation and ductility. Reinforcement strains were consistently lower in ZCC beams than in normal concrete beam, indicating improved bond performance. Failure was primarily governed by diagonal shear cracks at angles of 30–45°, similarly to NC beams but with more gradual crack development. The findings confirm that ZCC beams achieve shear performance comparable to beams made with conventional concrete while offering improved ductility and energy absorption, highlighting their potential as a sustainable alternative for shear-critical structural applications subjected to monotonic and cyclic loading.

Keywords: geopolymer (zero-cement) concrete; shear behavior; shear span-to-depth ratio; reinforcement ratio; monotonic loading; cyclic loading; diagonal cracks

Check for updates

Academic Editor: Constantin Chalioris

Received: 15 January 2026
Revised: 16 February 2026
Accepted: 21 February 2026
Published: 25 February 2026

Copyright: © 2026 by the authors. Licensee MDPI, Basel, Switzerland. This article is an open access article distributed under the terms and conditions of the Creative Commons Attribution (CC BY) license.

1. Introduction

Concrete remains the cornerstone of modern infrastructure, used extensively in buildings, bridges, and transportation systems worldwide. However, the environmental cost of

ordinary Portland cement (OPC), the primary binder in conventional concrete, is substantial. Cement production alone contributes approximately 7–8% of global anthropogenic CO_2 emissions, requires significant energy, and relies heavily on natural resources [1]. In response to these environmental challenges, zero-cement concrete (ZCC), also referred to as geopolymer or alkali-activated concrete, has emerged as a sustainable alternative [2]. ZCC replaces OPC with industrial by-products such as fly ash, ground granulated blast-furnace slag (GGBS), and red mud, activated by alkaline solutions, thereby reducing carbon emissions by up to 80% while maintaining comparable mechanical and durability properties [3–5].

The mechanical and durability performance of ZCC has been extensively documented. Studies demonstrate that ZCC exhibits high compressive and tensile strengths, superior chemical resistance, lower shrinkage and creep, and enhanced durability under aggressive conditions such as sulfate attack, chloride penetration, and freeze–thaw cycles [6,7]. Additionally, the inherent microstructural characteristics of geopolymer binders, including a dense matrix formation and a stronger interfacial transition zone, contribute to improved bond strength with reinforcement and enhanced long-term performance compared to OPC concrete [8]. Recent studies further support its potential: Hassoon and Qissab (2023) [9] critically reviewed the performance of fly ash-based ZCC, reporting that Class C FA yields higher compressive strength and performs well under ambient curing compared with Class F, with increased sodium hydroxide molarity enhancing strength; overall, FA-ZCC exhibits mechanical properties comparable to or slightly lower than normal concrete (NC), highlighting the need for standardized mix design methods. Hassoon and Al-Janabi (2024) [10] investigated 20 zero-cement reinforced concrete slabs under monotonic and impact loading, showing that ZCC slabs exhibit behavior comparable to that of conventional concrete with enhanced energy absorption and punching shear resistance, thereby confirming their suitability as sustainable, low-carbon structural alternatives. Similarly, Hassoon and Qissab (2024) [11] examined reinforced ZCC slabs under monotonic loading. It was observed that the increase in slab thickness and reducing bar spacing improve stiffness, load capacity, and energy absorption, with failure primarily governed by punching shear, thus demonstrating structural performance comparable to that of NC.

Experimental investigations on reinforced one-part geopolymer concrete beams have demonstrated shear responses comparable to OPC beams and confirmed the applicability of conventional shear design provisions under monotonic loading [12]. Specifically, Wan et al. [12] reported experimental-to-predicted shear strength ratios ($V_{u,exp}/V_{u,ACI}$) averaging approximately 1.15–1.30 for fly ash-based geopolymer beams with a/d ratios of 2.0–3.0 and longitudinal reinforcement ratios of 0.78–2.26%, indicating that ACI 318 provisions are conservative for geopolymer concrete. The present study confirms this trend, with experimental-to-predicted ratios averaging 1.39 across all tested configurations at a/d = 2.0, and further extends these findings to a broader range of compressive strengths (20–30 MPa) and reinforcement ratios (ρ = 0.0065–0.0141). A more recent study on geopolymer deep beams (Kannan et al. [13]) reported ultimate shear capacities approximately 18–25% higher than those of equivalent normal concrete specimens, with improved energy dissipation under monotonic loading. In the present study, ZCC beams achieved ultimate shear loads 5.5–10.1% higher than those of NC counterparts at comparable compressive strengths (20–30 MPa), with mid-span deflections 1.5–12.1% greater, confirming enhanced deformation capacity without a significant loss in stiffness.

Despite these advancements, most research has focused on the compressive, flexural, and durability performance of ZCC [14,15], while its shear behavior under realistic structural loading conditions remains understudied. Shear failure is particularly critical in beams, slabs, and frames, as it can lead to sudden and brittle collapse with minimal

warning, posing serious risks to structural safety [16]. A deeper understanding of shear performance is therefore essential for safe and reliable structural design, especially in shear-critical structural members.

Research specifically addressing the shear behavior of ZCC beams is relatively limited. Yacob et al. (2019) [17] observed that ZCC beams with varying shear span-to-depth ratios (a/d) exhibited diagonal cracking patterns similar to those of OPC beams, although crack propagation was more gradual and less abrupt. Akduman et al. (2023) [18] extended these findings by incorporating recycled construction and demolition waste aggregates into ZCC beams, showing that adequate reinforcement ratios could preserve shear strength comparable to that of conventional concrete. Investigations by Al-Jabali et al. [6] into red-mud-based alkali-activated beams showed ultimate shear strengths within 5–8% of OPC beams for ambient-cured specimens with $\rho \approx 1.0$–2.0% and $f'_c \approx 25$–35 MPa. The present work demonstrates a similar range of shear capacity ratios (ZCC/NC ≈ 1.05–1.10), while providing additional data on cyclic performance and the influence of three discrete reinforcement configurations (2Ø10, 3Ø10, 3Ø12) across two strength levels, an aspect not addressed in [6]. Recent numerical studies also suggest that the interaction between shear span-to-depth ratio, longitudinal reinforcement, and concrete compressive strength plays a significant role in governing failure modes, crack development, and energy absorption [8,19,20]. Tauqir et al. (2023) [21] examined the shear performance of geopolymer concrete slender beams and highlighted the influence of shear span and reinforcement ratio on failure mechanisms. However, experimental data on the combined monotonic and cyclic shear behavior of ZCC beams remain limited.

Cyclic and monotonic testing of geopolymer concrete beams by Jothivel and Basil Ahamed [22] revealed stable hysteresis loops and cumulative energy absorption approximately 10–20% higher than that of OPC beams under equivalent displacement cycles. The present study reports energy absorption advantages of 5–48% for ZCC beams over NC beams under cyclic loading, a substantially wider performance range, attributed to the systematic variation of reinforcement ratio and compressive strength investigated herein, parameters that were not simultaneously varied in [22]. Yacob et al. (2019) [17] reported that the shear and flexural performance of cyclically loaded geopolymer beams were nearly equivalent to those of OPC beams, while stiffness degradation and crack propagation occurred more gradually, indicating improved damage tolerance. These findings suggest that ZCC can provide superior resilience under repeated load cycles, which is particularly relevant for structures in seismic zones or for transportation infrastructure subjected to dynamic loading.

Comparative studies of ZCC and conventional concrete beams under realistic shear loading scenarios remain scarce, and systematic evaluations that simultaneously examine multiple design parameters are still lacking. Hence, the objective of this study is to examine the combined effects of concrete compressive strength, reinforcement ratio, and shear span-to-depth ratio on beam performance under both monotonic and cyclic loading.

Although shear resistance in reinforced concrete is largely governed by aggregate interlock and compressive strength, differences in binder chemistry and microstructure may influence shear transfer mechanisms after cracking. Previous studies have reported that geopolymer binders form a denser matrix and a stronger interfacial transition zone with aggregates and steel reinforcement compared to ordinary Portland cement systems. Consequently, this study does not presuppose higher shear strength for zero-cement concrete but aims to experimentally assess whether improved bond characteristics and crack control affect the shear response and post-cracking behavior when aggregate type and compressive strength are kept comparable. The present study addresses these gaps by experimentally investigating a large comprehensive set of simply supported ZCC beams

under monotonic and cyclic loading. The study also evaluates the influence of compressive strength, reinforcement ratio, and shear span-to-depth ratio on shear capacity, ductility, and energy dissipation, while providing direct performance comparisons with conventional concrete beams.

2. Materials and Methodology

An experimental program was conducted to evaluate the shear performance of ZCC beams under monotonic and cyclic loading. Figure 1 illustrates the research workflow where it was designed to investigate the influence of three primary parameters on the structural behavior of reinforced concrete beams: concrete compressive strength, shear span-to-depth ratio (a/d), and reinforcement ratio (ρ), on the structural behavior of reinforced concrete beams. Conventional normal concrete (NC) beams were included as control specimens to provide a direct performance benchmark for ZCC.

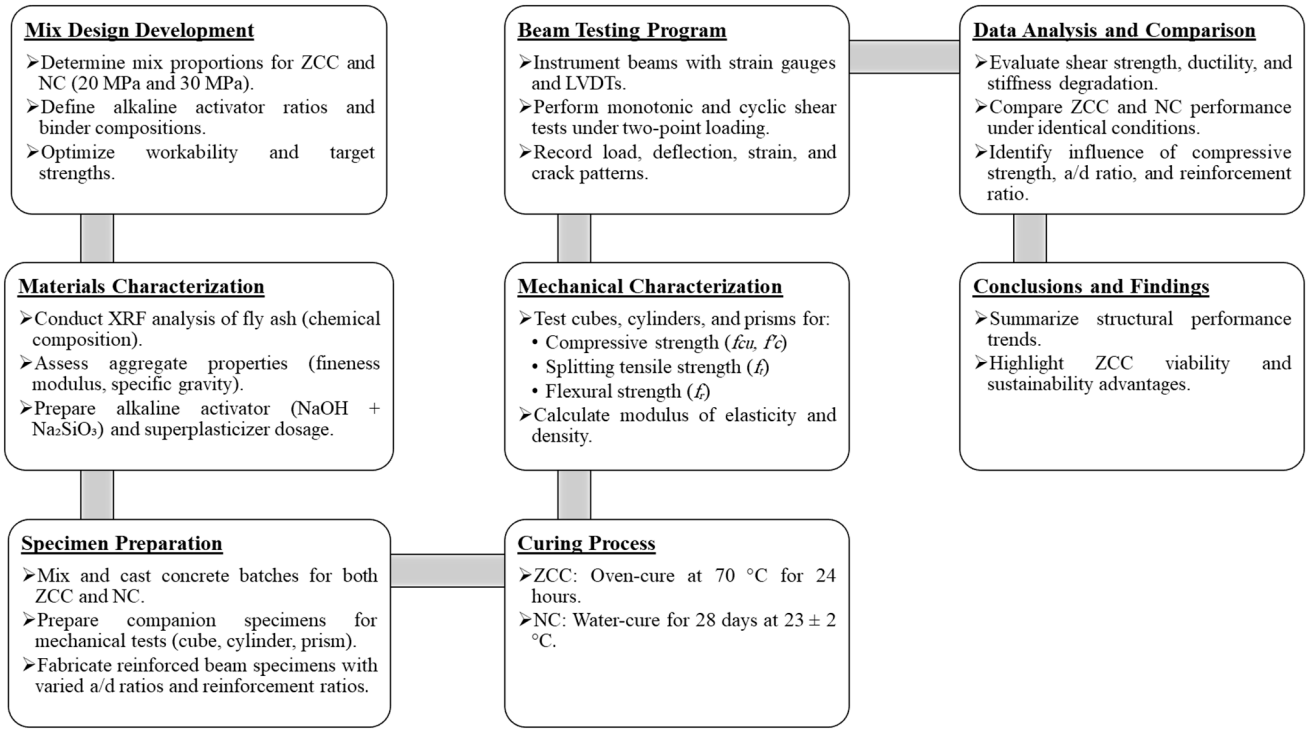


Figure 1. Research workflow and experimental program.

The ZCC mixtures were produced by fully replacing OPC with low-calcium Class F fly ash as the sole binder. The fly ash, obtained from a local thermal power plant, was analyzed using X-ray fluorescence (XRF), which indicated a combined silica, alumina, and iron oxide content exceeding 75% and a calcium-oxide content below 10%, confirming its classification as a low-calcium pozzolanic material in accordance with ASTM C618 [23,24]. The fly ash had a specific gravity of 2.25 and a median particle size of approximately 12 µm.

The alkali activator consisted of sodium hydroxide (NaOH) and sodium silicate (Na_2SiO_3) solutions. Analytical-grade NaOH pellets were dissolved in distilled water to prepare a 10 M solution, which was aged for 24 h prior to mixing to ensure chemical stability. The sodium silicate solution, containing approximately 29.4% SiO_2, 14.7% Na_2O, and 55.9% H_2O, had a silica modulus (SiO_2/Na_2O) of approximately 2.5. These solutions were combined at a mass ratio of 2:1 (Na_2SiO_3: NaOH) to optimize the geopolymerization reaction and produce a workable mix. The ratio of alkaline activator to fly ash (AAL/FA) was adjusted to achieve target compressive strengths of 20 MPa and 30 MPa.

Natural river sand with a fineness modulus of 2.6 and specific gravity of 2.62 was used as fine aggregate, while crushed granite with a maximum nominal size of 12 mm and specific gravity of 2.70 was used as the coarse aggregate. A polycarboxylate-based superplasticizer (Sika ViscoCrete-180GS, SIKA IRAQ, Erbil, Iraq) was added at 1.2% of the binder weight to enhance workability and ensure uniform dispersion of particles throughout the mixture.

For the NC control mixtures, OPC (ASTM Type I) was used as the binder, and the same aggregates and superplasticizer used in the ZCC mixtures were incorporated to ensure consistency. The water-to-cement ratio (w/c) was fixed at 0.45, and the mix proportions were adjusted to produce compressive strengths comparable to those of the ZCC mixtures (20 MPa and 30 MPa). The detailed mix proportions are summarized in Table 1.

Table 1. Mix proportions of ZCC and NC mixtures (per 1 m^3 of concrete).

Mix ID	Fly Ash (kg)	OPC (kg)	10 M NaOH Solution (kg)	Na_2SiO_3 (kg)	Sand (kg)	Coarse Agg. (kg)	Free Water (kg)	SP (% Binder)
ZCC-20	400	-	45	90	680	1050	-	1.2
ZCC-30	400	-	45	90	670	1040	-	1.2
NC-20	-	400	-	-	690	1060	180	1.2
NC-30	-	420	-	-	680	1050	175	1.2

Water in ZCC mixtures is included as part of the alkaline activator solutions (10 M NaOH and Na_2SiO_3), and no additional free water was added.

A total of 48 reinforced concrete beams were cast and tested under monotonic and cyclic two-point loading until failure; six beams were NC control specimens, and the remaining 42 beams were ZCC, designed to evaluate the structural response under both monotonic and cyclic loading conditions. Each beam measured 1400 mm in length, 200 mm in depth, and 150 mm in width, and was simply supported with a clear span of 1200 mm. The reinforcement configurations of the beams are illustrated in Figure 2. The beams were divided into groups according to concrete compressive strength (20 MPa and 30 MPa), longitudinal reinforcement detailing (2Ø10, 3Ø10, and 3Ø12), and shear span-to-effective depth ratio (a/d = 2, 2.5, and 3). The same longitudinal reinforcement was used at the upper and lower faces for beams subjected to cyclic loading.

Strain gauges were attached at mid-span on both the tensile longitudinal reinforcement and the concrete surface near the shear span to record steel and concrete strains, respectively. Mid-span deflection was measured using Linear Variable Differential Transformers (LVDTs), as illustrated in Figure 3.

For monotonic loading, a displacement-controlled rate of 0.5 mm/min was applied until failure. Figure 4 illustrates the overall experimental setup. For cyclic loading, the load was applied in successive cycles up to a predetermined fraction of the ultimate monotonic load, with controlled unloading to simulate repeated service conditions, as shown in Figure 5. The cyclic loading protocol is illustrated schematically in Figure 6.

The mechanical properties of both ZCC and NC mixtures were determined using companion specimens tested under compression, tension, and flexure, as summarized in Table 2. The mechanical properties include compressive strength determined on both cubes (f_{cu}) and cylinders (f'_c), where f'_c denotes compressive strength, f_t represents splitting tensile strength, and f_r corresponds to flexural strength. The results show that ZCC achieved mechanical strengths comparable to, or slightly exceeding, those of NC, highlighting the structural viability of the zero-cement system.

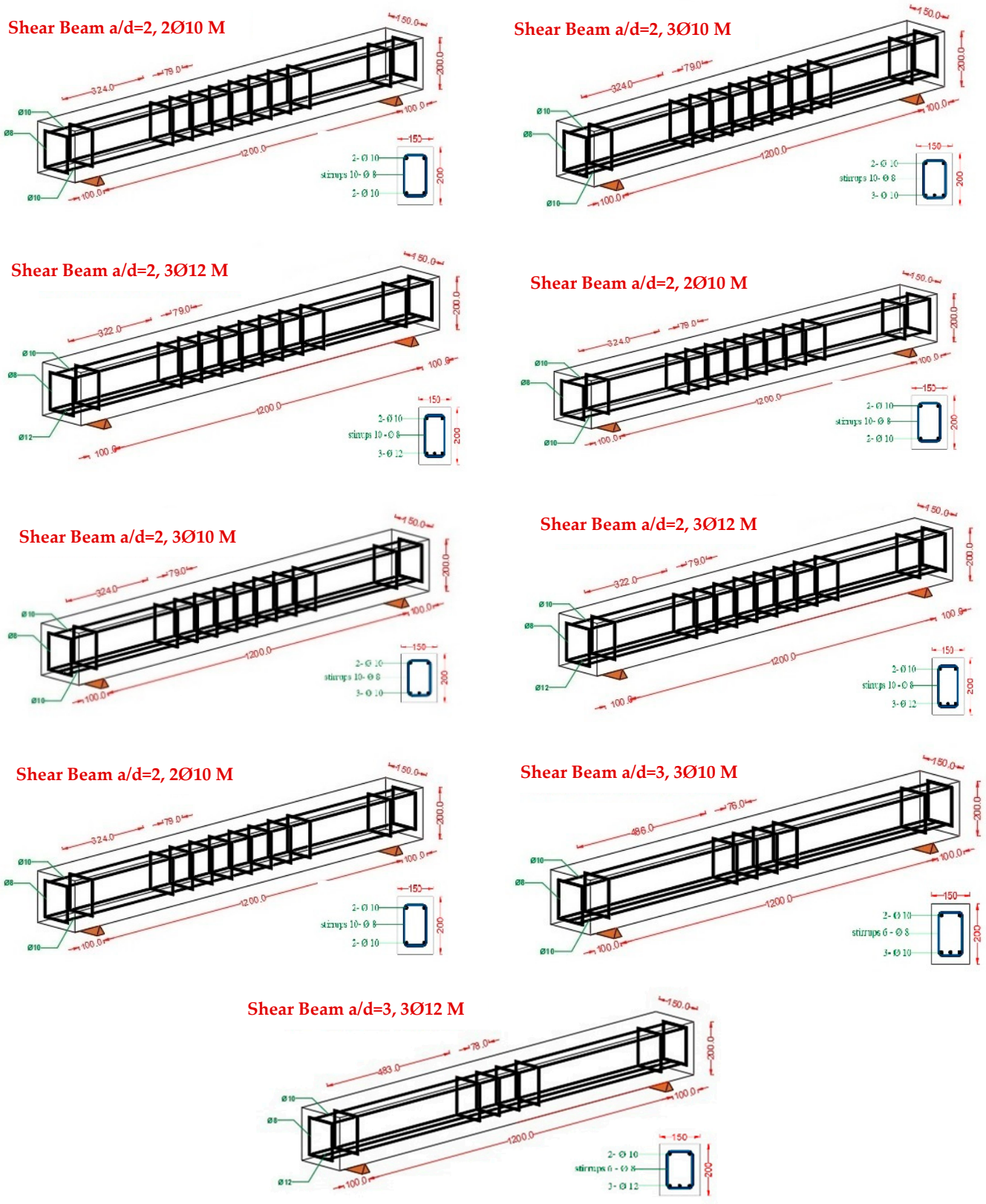


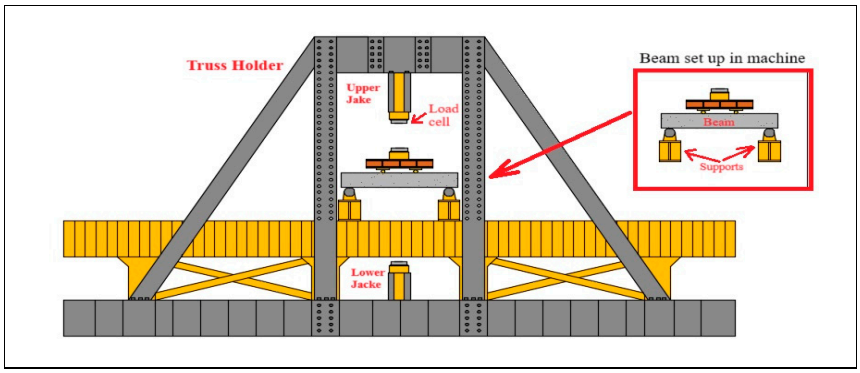
Figure 2. Reinforcement layout.



Figure 3. LVDT and instrumentation setup for mid-span deflection measurement (visible elements at mid-span correspond to sensor wiring and not flexural cracking).



(**a**)

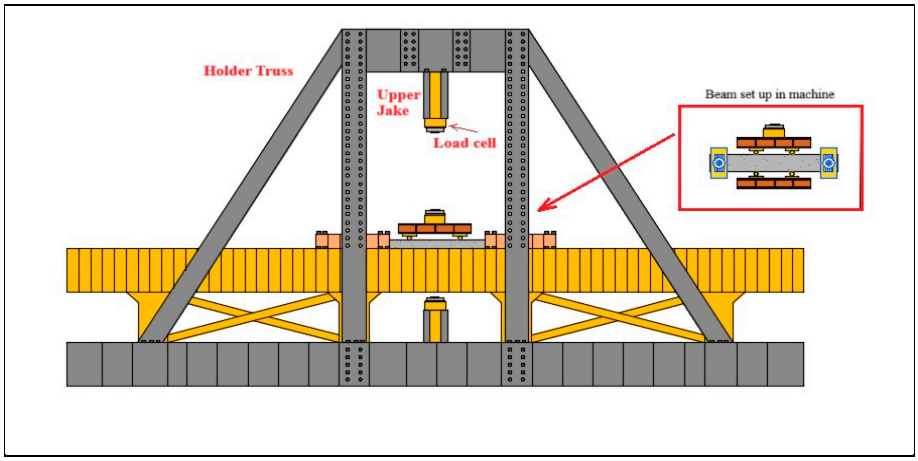


(**b**)

Figure 4. (**a**) Specimen in the testing machine, (**b**) Schematic diagram for the monotonic test setup.



(**a**) (**b**)



(**c**)

Figure 5. Test setup for cyclic loading (**a**) front view, (**b**) side view, and (**c**) schematic diagram of the test setup.

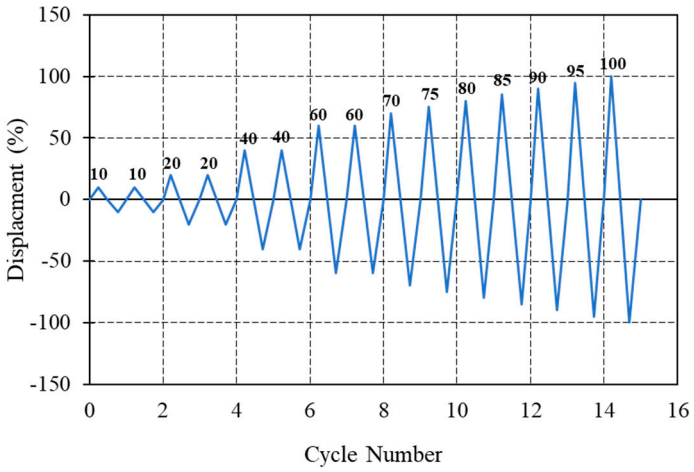


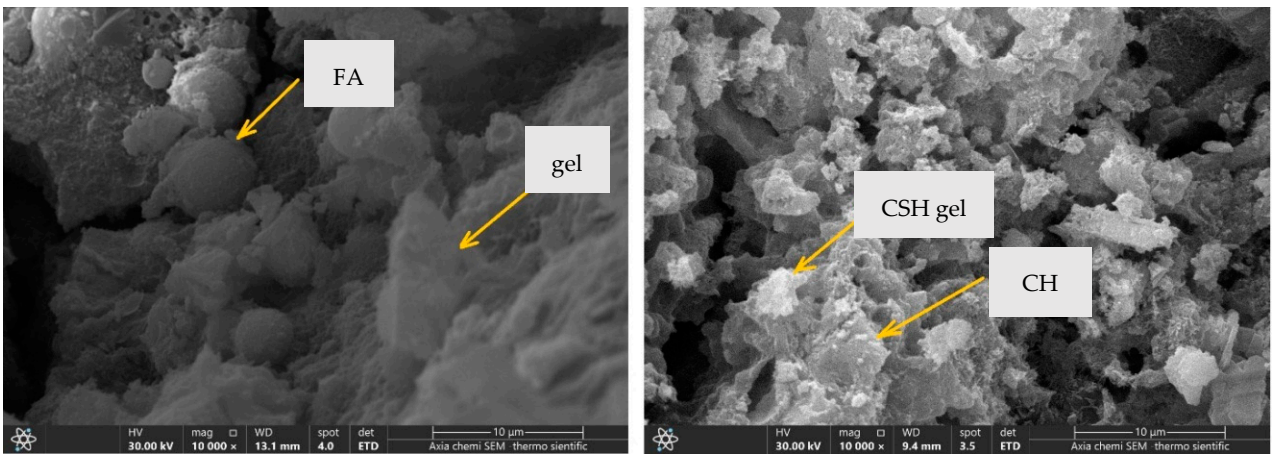
Figure 6. Testing cyclic loading protocol.

Table 2. Mechanical properties of the ZCC and NC mixtures at 28 days.

Concrete Type	f_{cu} (MPa)	f'_c (MPa)	f_t (MPa)	f_r (MPa)
NC-20	24.32	21.89	2.02	3.06
NC-30	36.03	32.07	2.92	3.71
ZCC-20	26.90	23.94	2.53	3.11
ZCC-30	37.37	34.38	3.06	4.04

The measured mechanical properties of the ZCC mixtures are consistent with values reported in recent studies. Previous investigations on fly ash-based geopolymer concretes have reported compressive strengths in the range of 18–35 MPa, splitting tensile strengths of 1.6–3.2 MPa, and elastic moduli between 18 and 28 GPa. The present results fall well within these ranges, confirming the reliability of the adopted mix design, curing procedure, and testing methodology.

Scanning electron microscopy (SEM) analysis was conducted as a qualitative supplementary observation to provide microstructural context for the macroscopic structural trends reported in this study. The micrographs in Figure 7 qualitatively show that ZCC possesses a denser and more homogeneous matrix with fewer visible pores compared to NC. As EDX elemental mapping was not conducted within the scope of this study, phase identification is necessarily qualitative; observed binding phases are described generically as geopolymer reaction products for ZCC and C-S-H-type phases for NC, consistent with the established literature on fly ash-based geopolymer systems, where EDX analyses have confirmed Si/Al molar ratios in the range of 1.5–2.5 and the formation of a dense aluminosilicate gel network [3–5]. These observations support, but do not independently confirm, the improved bond behavior and energy dissipation of ZCC documented at the structural level. Future work should incorporate multi-magnification SEM imaging and EDX elemental mapping to enable quantitative phase identification and to more rigorously correlate microstructural characteristics with macroscopic shear response.



(**a**) (**b**)

Figure 7. SEM micrographs comparing (**a**) NC and (**b**) ZCC.

The experimental procedure and test parameters were established to isolate the primary variables governing shear behavior in reinforced concrete beams while ensuring relevance to practical structural applications. Two compressive strength levels (20 and 30 MPa) were selected to represent typical strength classes used in conventional structural concrete and to enable a direct comparison between ZCC and NC. The longitudinal rein-

forcement ratios were varied within practical design limits to examine their influence on shear transfer mechanisms, stiffness, ductility, and energy dissipation.

The shear span-to-effective depth ratios (a/d = 2.0, 2.5, and 3.0) were chosen to capture the transition from shear-dominated to flexure-influenced behavior, as widely recognized in reinforced concrete beam mechanics. Monotonic loading was applied to establish baseline strength, stiffness, and failure modes, while cyclic loading protocols were adopted to simulate repeated loading effects relevant to seismic and fatigue conditions. This systematic parameter selection allows a consistent evaluation of shear response and ensures that observed differences are attributable to material type and structural configuration rather than experimental bias.

3. Results and Discussion

3.1. Monotonic Loading

A total of 24 beams were tested under monotonic two-point loading to evaluate the load–deflection and shear response of ZCC in comparison with NC. The specimens were divided into groups based on compressive strength (f'_c = 20 and 30 MPa), reinforcement ratios (ρ = 0.0065, 0.0097, and 0.0141, corresponding to 2Ø10, 3Ø10, and 3Ø12, respectively), and shear span-to-effective depth ratios (a/d = 2, 2.5, and 3). Six NC and six ZCC beams were tested for each strength level with a/d = 2 under identical conditions. Figure 8 shows the comparison of ultimate load capacities for NC and ZCC beams at both strength levels (20 and 30 MPa). It can be observed that ZCC beams exhibited ultimate loads comparable to, or slightly higher, than those of NC beams, confirming that replacing OPC with fly ash–based binder did not compromise structural performance. ZCC beams exhibited higher shear capacity compared to NC beams; however, it should be noted that the compressive strength of ZCC specimens was approximately 7–9% higher than that of NC. Accordingly, part of the observed increase in shear capacity can be attributed to this strength difference, while the remaining enhancement may be associated with improved bond characteristics and post-cracking behavior of the geopolymer matrix.

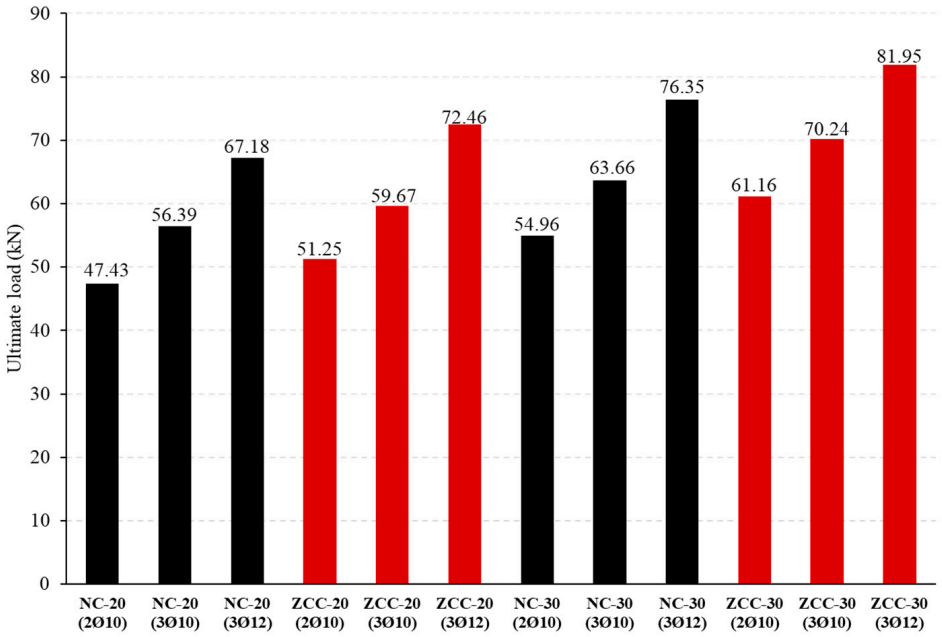


Figure 8. Ultimate load for NC and ZCC (f'_c = 20 MPa and 30 MPa).

For beams with a compressive strength of 20 MPa, the ultimate load capacities of ZCC beams increased by approximately 7.45%, 5.50%, and 7.29%, while the corresponding

mid-span deflections increased by 6.06%, 5.36%, and 10.18% for beams reinforced with 2Ø10, 3Ø10, and 3Ø12 bars, respectively, compared to NC. At 30 MPa, the ZCC beams exhibited ultimate load increases of 10.14%, 9.37%, and 6.83%, with deflection increments of 1.49%, 5.57%, and 12.12% for the same reinforcement configurations, as presented in Table 3. In Table 3, P_{cr} represents the first cracking load (kN), Δ_{cr} is the corresponding deflection at first crack (mm), P_u denotes the ultimate load at failure (kN), Δ_u is the ultimate mid-span deflection (mm), and K denotes the overall stiffness of the beam (kN/mm), while P_{cr}/P_u and Δ_{cr}/Δ_u indicate the ratios of cracking to ultimate load and deflection, respectively. An analytical comparison is also conducted herein to compare the experimental cracking shear loads with those obtained from Equation (b) in Table 22.5.5.1 of the ACI 318-19 [25], as presented in Table 3. The results indicate that the ACI formula is conservative with respect to cracking shear load calculated for the (a/d = 2.0) case for all specimens with an average ($P_{cr(Exp.)}/P_{cr(ACI)}$ of 1.39. Figures 9 and 10 illustrate the load–deflection response of the tested beams. Observations regarding cracking patterns are therefore based on experimental inspection rather than these figures, and both ZCC and NC beams exhibited similar diagonal shear cracking prior to failure. In general, ZCC beams exhibited comparable or higher ductility than NC beams; however, the NC-20 (2Ø10) specimen showed slightly higher ductility than its ZCC counterpart. This improved performance is attributed to the dense geopolymeric matrix and enhanced bond between aggregates and binder, which reduce material brittleness and improve post-cracking strength retention.

Table 3. Experimental results for beams NC20 and ZCC20 under monotonic loading (a/d = 2).

Group	$P_{cr(Exp.)}$ (kN)	$P_{cr(ACI)}$ (kN)	$P_{cr(Exp.)}/P_{cr(ACI)}$	Δ_{cr} (mm)	P_u (kN)	Δ_u (mm)	K (kN/mm)	P_{cr}/P_u %	Δ_{cr}/Δ_u %	Energy Absorption (kN.mm)
NC-20 (2Ø10)	17.24	14.00	1.23	1.93	47.43	8.49	7.12	36.35	22.73	248.95
NC-20 (3Ø10)	20.28	16.00	1.27	2.10	56.39	7.11	9.40	36.00	29.54	250.56
NC-20 (3Ø12)	27.80	18.13	1.53	2.36	67.18	6.88	10.09	41.38	34.30	276.94
ZCC-20 (2Ø10)	19.67	14.65	1.34	2.28	51.25	8.46	7.23	38.38	26.95	267.53
ZCC-20 (3Ø10)	25.10	16.74	1.50	2.52	59.67	7.28	9.41	42.06	34.62	289.65
ZCC-20 (3Ø12)	28.94	18.96	1.53	2.56	72.46	7.30	12.10	40.00	35.07	318.40
NC-30 (2Ø10)	20.40	16.95	1.20	1.93	54.96	7.01	9.22	37.11	27.53	232.91
NC-30 (3Ø10)	28.32	19.37	1.46	2.06	63.66	6.19	11.72	44.48	33.27	242.00
NC-30 (3Ø12)	31.83	21.94	1.45	1.22	76.35	5.28	17.55	41.69	23.11	272.58
ZCC-30 (2Ø10)	21.50	17.55	1.23	2.04	61.16	7.28	10.11	35.15	28.02	265.77
ZCC-30 (3Ø10)	29.28	20.05	1.46	2.29	70.24	6.96	12.22	41.68	32.90	299.84
ZCC-30 (3Ø12)	35.67	22.72	1.57	1.39	81.95	5.62	16.56	43.53	24.73	316.22

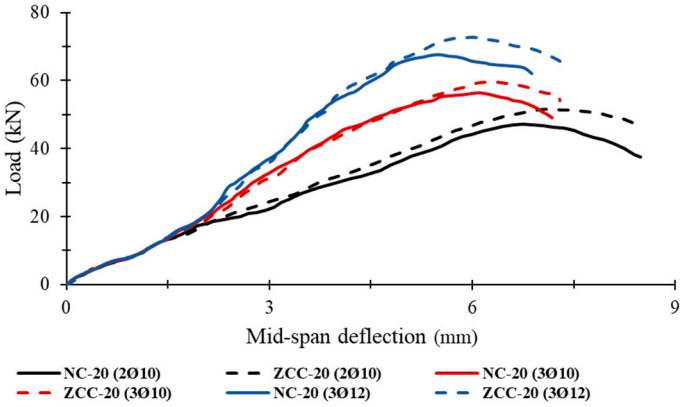


Figure 9. Mid-span load–deflection curves for NC and ZCC (f'_c = 20 MPa; 2Ø10, 3Ø10, and 3Ø12 reinforcement).

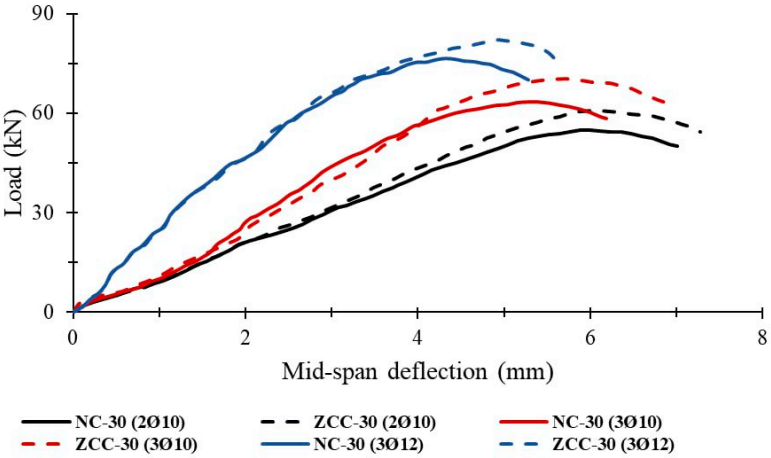


Figure 10. Mid-span load–deflection curves for NC and ZCC (f'_c = 30 MPa; 2Ø10, 3Ø10, and 3Ø12 reinforcement).

To investigate the effect of the shear span-to-depth ratio, additional beams were tested at a/d = 2.5 and 3. The load–deflection curves for a/d = 2.5 are shown in Figure 11, and the corresponding results are presented in Table 4. Increasing the compressive strength from 20 to 30 MPa resulted in ultimate load increases of 17.47%, 15.83%, and 12.46% for beams reinforced with 2Ø10, 3Ø10, and 3Ø12 bars, respectively. Meanwhile, the ultimate deflection decreased by 11.78%, 9.48%, and 14.94%, indicating that higher compressive strength enhances stiffness and reduces deformation. Table 4 also reports that the cracking shear loads calculated according to equation (b) in Table 22.5.5.1 of the ACI 318-19 [25] are conservative, with an average $P_{cr(Exp.)}/P_{cr(ACI)}$ of 1.37.

Table 4. Experimental results for beams ZCC-20 and ZCC-30 under monotonic loading (a/d = 2.5).

Group	P_{cr} (kN)	$P_{cr(ACI)}$ (kN)	$P_{cr(Exp.)}/P_{cr(ACI)}$	Δ_{cr} (mm)	P_u (kN)	Δ_u (mm)	K (kN/mm)	P_{cr}/P_u %	Δ_{cr}/Δ_u %	Energy Absorption (kN.mm)
ZCC-20 (2Ø10)	20.39	14.65	1.39	3.81	38.12	10.74	4.10	53.50	35.47	259.83
ZCC-20 (3Ø10)	24.90	16.74	1.49	3.90	47.34	10.20	5.54	52.60	38.24	298.83
ZCC-20 (3Ø12)	27.51	18.96	1.45	3.58	56.86	9.82	7.11	48.40	36.46	338.94

Table 4. *Cont.*

Group	P_{cr} (kN)	$P_{cr(ACI)}$ (kN)	$P_{cr(Exp.)}/P_{cr(ACI)}$	Δ_{cr} (mm)	P_u (kN)	Δ_u (mm)	K (kN/mm)	P_{cr}/P_u %	Δ_{cr}/Δ_u %	Energy Absorption (kN.mm)
ZCC-30 (2Ø10)	21.56	17.55	1.23	2.80	46.19	9.33	5.55	46.70	30.00	276.77
ZCC-30 (3Ø10)	26.25	20.05	1.31	2.83	56.24	8.83	7.20	46.70	32.05	312.39
ZCC-30 (3Ø12)	31.07	22.72	1.37	2.87	64.95	7.86	9.33	47.84	36.51	329.27

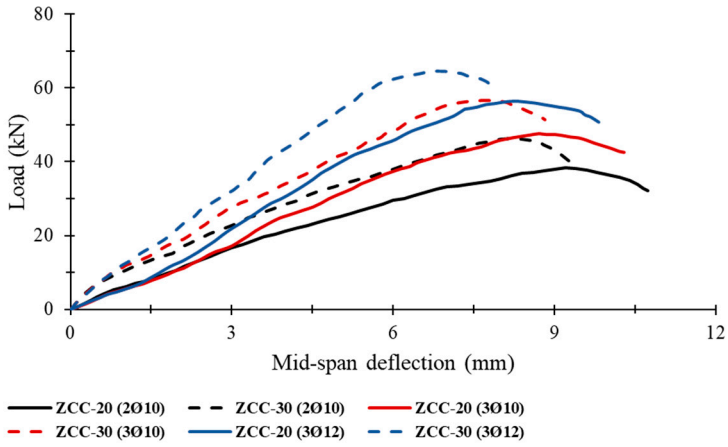


Figure 11. Mid-span load–deflection curves for ZCC-20 and ZCC-30 with a/d = 2.5.

For a/d = 3, the beams exhibited a more flexure-dominated behavior due to the increased span length. The mid-span load–deflection curves shown in Figure 12 and the test results listed in Table 5 indicate that, when the compressive strength was increased from 20 to 30 MPa, the ultimate load capacities improved by 15.94%, 13.94%, and 12.36%, while the corresponding deflections decreased by 10.91%, 4.70%, and 16.54% for the 2Ø10, 3Ø10, and 3Ø12 reinforcements, respectively. The improvement in load capacity at higher strength is mainly attributed to the increased material stiffness and improved stress transfer efficiency between the steel reinforcement and the surrounding geopolymeric matrix.

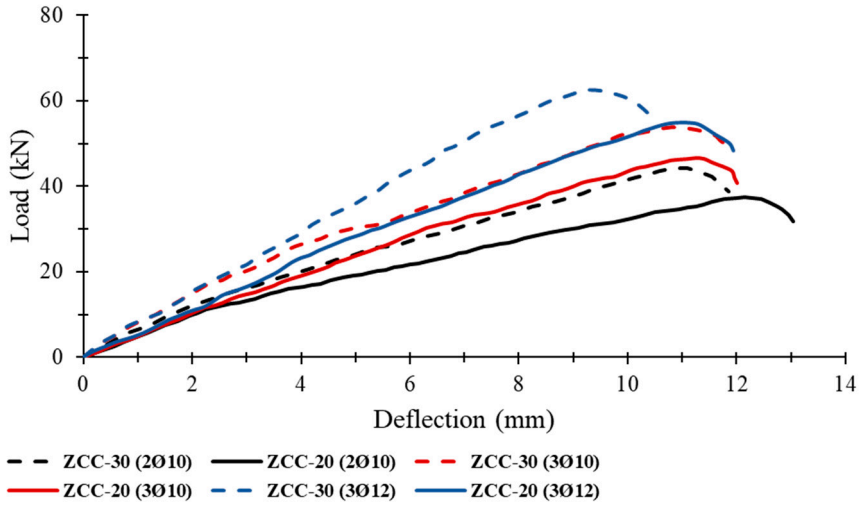


Figure 12. Mid-span load–deflection curves for ZCC-20 and ZCC-30 with a/d = 3.

Table 5. Experimental results for beams ZCC-20 and ZCC-30 under monotonic loading (a/d = 3).

Group	P_{cr} (kN)	$P_{cr(ACI\text{-}19)}$ (kN)	$P_{cr(Exp.)}/P_{cr(ACI\text{-}19)}$	Δ_{cr} (mm)	P_u (kN)	Δ_u (mm)	K (kN/mm)	P_{cr}/P_u %	Δ_{cr}/Δ_u %	Energy Absorption (kN.mm)
ZCC-20 (2Ø10)	13.53	14.65	0.92	3.15	37.56	12.95	3.05	36.02	24.32	290.97
ZCC-20 (3Ø10)	15.11	16.74	0.90	3.30	46.12	11.97	4.06	32.76	27.60	318.57
ZCC-20 (3Ø12)	22.17	18.96	1.17	3.83	55.15	11.95	5.02	40.20	32.05	375.20
ZCC-30 (2Ø10)	15.97	17.55	0.91	2.95	44.68	11.85	4.03	35.74	24.89	315.52
ZCC-30 (3Ø10)	19.01	20.05	0.95	2.70	53.59	11.88	4.93	35.47	22.73	345.49
ZCC-30 (3Ø12)	29.01	22.72	1.28	4.00	62.93	10.29	6.67	46.10	38.87	385.26

Notably, the reported cracking shear loads calculated according to ACI 318-19 [25] are slightly greater than the test results for most cases, indicating that the ACI formula is less conservative for this case when compared to the other cases. However, the average $P_{cr(Exp.)}/P_{cr(ACI)}$ for this case is 1.02.

The influence of the a/d ratio was further analyzed for all beam groups to understand its role in the transition between shear and flexural behavior. Increasing the a/d ratio from 2 to 2.5 caused the ultimate load capacity to decrease by 24.89–34.44%, while deflection increased by 23.76–28.88%. When a/d was further increased from 2 to 3, the ultimate load decreased by 29.38–36.88%, and the deflection increased by 42.36–47.51%, as shown in Table 6. The observed decrease in ultimate load with increasing shear span-to-effective depth ratio (a/d) agrees with established reinforced concrete behavior. As a/d increased from 2 to 3, both ZCC and NC beams exhibited reduced shear capacity and increased deflection, indicating a shift from shear-dominated to flexure-dominated response. The similar trends observed in ZCC and NC beams confirm that zero-cement concrete follows conventional shear transfer mechanisms. These trends indicate that larger shear spans reduce the contribution of shear stresses, promoting a shift from shear to flexural response and resulting in higher bending-induced deflection and reduced overall stiffness. The corresponding load–deflection curves (Figures 13–15) clearly depict this transition, where beams with a/d = 3 exhibited wider cracks, larger deflections, and more pronounced ductile flexural failure modes compared to those with a/d = 2.

Table 6. Comparative results of shear span-to-depth ratio for ZCC-20 and ZCC-30 beams (a/d = 2, 2.5, and 3).

Group	*a/d*	Difference in Ultimate Load %	Difference in Ultimate Deflection %
ZCC-20 (2Ø10)	2.5 to 2	−34.44 *	23.76
	3 to 2.5	−1.49	24.39
	3 to 2	−36.45	42.36
ZCC-30 (2Ø10)	2.5 to 2	−32.41	27.28
	3 to 2.5	−3.38	24.98
	3 to 2	−36.88	45.45

Table 6. *Cont.*

Group	*a/d*	Difference in Ultimate Load %	Difference in Ultimate Deflection %
ZCC-20 (3Ø10)	2.5 to 2	−26.05	25.85
	3 to 2.5	−2.65	24.80
	3 to 2	−29.38	44.24
ZCC-30 (3Ø10)	2.5 to 2	−24.89	26.38
	3 to 2.5	−4.94	28.08
	3 to 2	−31.07	47.05
ZCC-20 (3Ø12)	2.5 to 2	−27.44	25.13
	3 to 2.5	−3.10	27.21
	3 to 2	−31.39	45.50
ZCC-30 (3Ø12)	2.5 to 2	−26.17	28.88
	3 to 2.5	−3.21	26.19
	3 to 2	−30.22	47.51

* The minus signs indicate a decrease in the ultimate load.

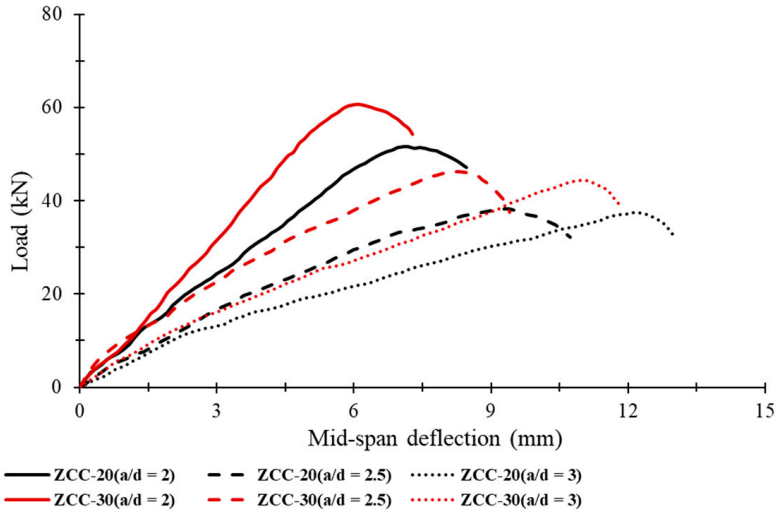


Figure 13. Mid-span load–deflection curves for ZCC-20 and ZCC-30 with 2Ø10 reinforcement.

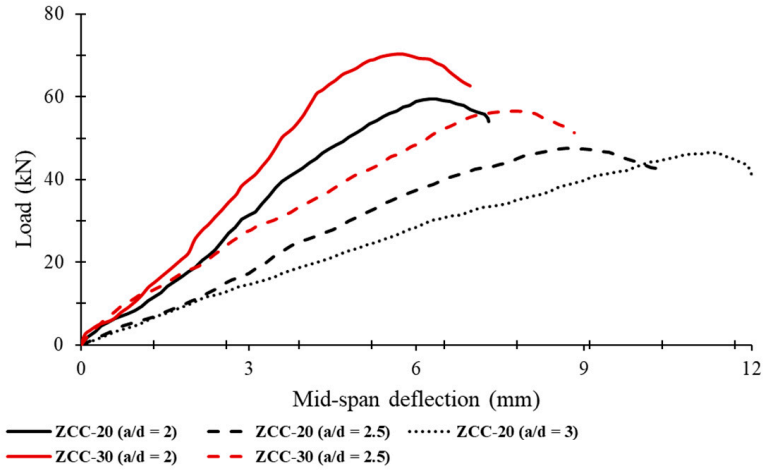


Figure 14. Mid-span load–deflection curves for ZCC-20 and ZCC-30 with 3Ø10 reinforcement.

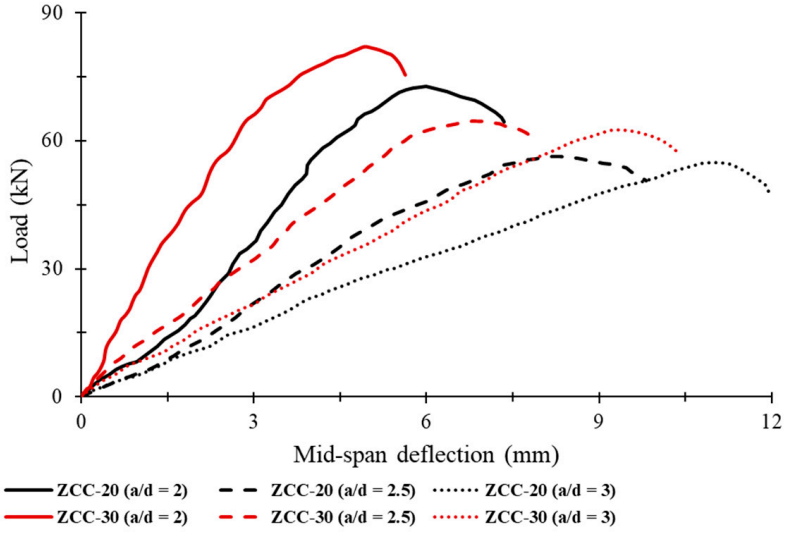


Figure 15. Mid-span load–deflection curves for ZCC-20 and ZCC-30 with 3Ø12 reinforcement.

Consequently, the results confirm that under monotonic loading, ZCC beams achieved comparable or slightly superior flexural performance compared to NC beams. ZCC specimens exhibited up to 10–16% higher ultimate loads, greater ductility, and enhanced energy absorption capacity. Increasing compressive strength improved stiffness and load capacity, while larger shear spans led to reduced capacity and increased deflection due to the greater dominance of flexural action. Despite the absence of cement, ZCC maintained stable cracking behavior and ductile failure, demonstrating its structural reliability and potential as a sustainable alternative to conventional concrete.

3.2. Cyclic Loading

Cyclic loading tests were conducted to evaluate the shear response of ZCC and NC beams with varying reinforcement ratios, compressive strengths, and shear span-to-depth ratios (a/d). The loading regime involved repeated load-unload-reload cycles applied through a servo-controlled testing system. The applied load, mid-span deflection, and number of cycles to failure were recorded using load cells and LVDTs. Cyclic loading generally resulted in reduced load-carrying capacity and stiffness compared with monotonic loading, as repeated stress reversals induced microstructural degradation in both the concrete matrix and steel reinforcement. The progressive accumulation of microcracks led to incremental stiffness deterioration and lower ultimate load capacity. Most specimens failed between cycles 11 and 13, corresponding to approximately 80–90% of the ultimate deflection observed under monotonic loading.

The comparative performance of ZCC and NC beams with a shear span-to-depth ratio (a/d = 2) is summarized in Table 7 and illustrated in Figures 16–19. For beams with f'_c = 20 MPa, the ultimate load capacity of ZCC increased by about 9.97%, 13.62%, and 13.31%, while deflection increased by 3.71%, 10.15%, and 4.26% for reinforcement ratios corresponding to 2Ø10, 3Ø10, and 3Ø12, respectively. At a higher compressive strength of 30 MPa, the ultimate load capacity rose by 9.78%, 11.09%, and 1.99%, accompanied by deflection increases of 1.80%, 17.03%, and 1.51% for the same reinforcement ratios. The load–deflection hysteresis curves (Figures 16–19, the small red circles in the figures indicate the failure points) demonstrate stable cyclic performance with limited degradation of stiffness across cycles. These results confirm that ZCC beams exhibited comparable or slightly superior behavior to NC beams, maintaining ductile and energy-absorbing characteristics even under repeated loading.

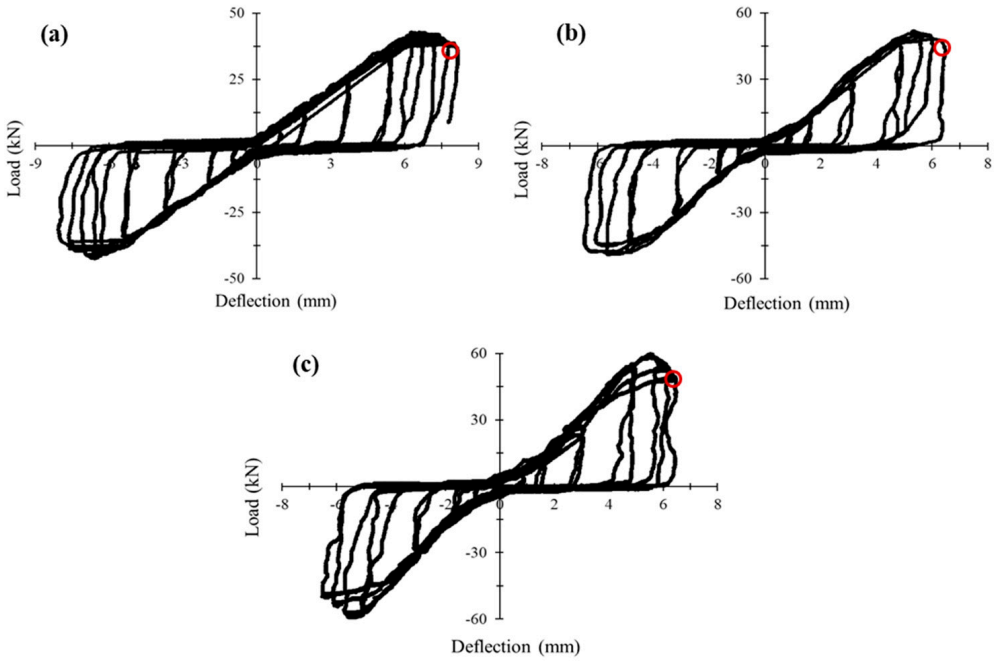


Figure 16. Load–deflection hysteresis curve for NC-20 with a/d = 2: (**a**) (2Ø10), (**b**) (3Ø10), (**c**) (3Ø12).

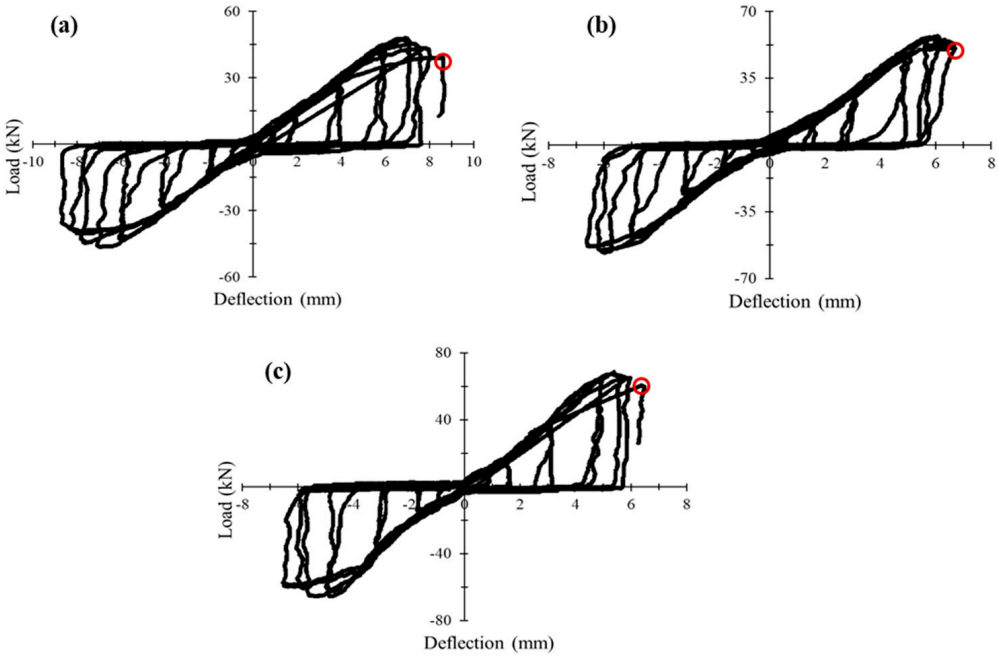


Figure 17. Load–deflection hysteresis curve for ZCC-20 with a/d = 2: (**a**) (2Ø10), (**b**) (3Ø10), (**c**) (3Ø12).

Table 7. Experimental results for beams NC-20, NC-30, ZCC-20, and ZCC-30 under cyclic loading with a/d = 2.

Group	ρ	P_u (kN)	Δ_u (mm)	K (kN/mm)	No. of Cycles to Failure	Energy Absorption (kN.mm)
NC-20 (2Ø10)	0.0065	42.18	6.75	6.25	13	1256.37
NC-20 (3Ø10)	0.0097	48.77	5.49	8.88	11	1638.43
NC-20 (3Ø12)	0.0141	59.59	5.39	11.06	11	1695.8
ZCC-20 (2Ø10)	0.0065	46.85	7.01	6.68	12	2121.59

Table 7. *Cont.*

Group	ρ	P_u (kN)	Δ_u (mm)	K (kN/mm)	No. of Cycles to Failure	Energy Absorption (kN.mm)
ZCC-20 (3Ø10)	0.0097	56.46	6.11	9.24	11	2306.43
ZCC-20 (3Ø12)	0.0141	68.74	5.63	12.2	11	2476.81
NC-30 (2Ø10)	0.0065	52.04	5.47	9.51	11	1182.71
NC-30 (3Ø10)	0.0097	57.55	4.53	12.7	13	1885.46
NC-30 (3Ø12)	0.0141	73.88	3.91	18.9	11	2053.5
ZCC-30 (2Ø10)	0.0065	57.68	5.57	10.4	11	1724.94
ZCC-30 (3Ø10)	0.0097	65.21	5.46	11.9	11	1849.63
ZCC-30 (3Ø12)	0.0141	75.38	3.97	19	11	1959.96

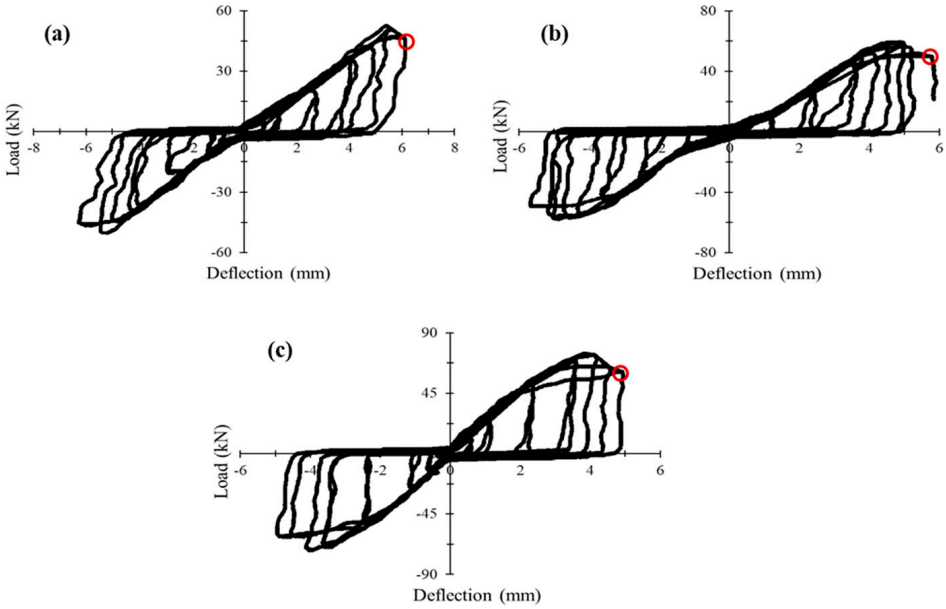


Figure 18. Load–deflection hysteresis curve for NC-30 with a/d = 2: (**a**) (2Ø10), (**b**) (3Ø10), (**c**) (3Ø12).

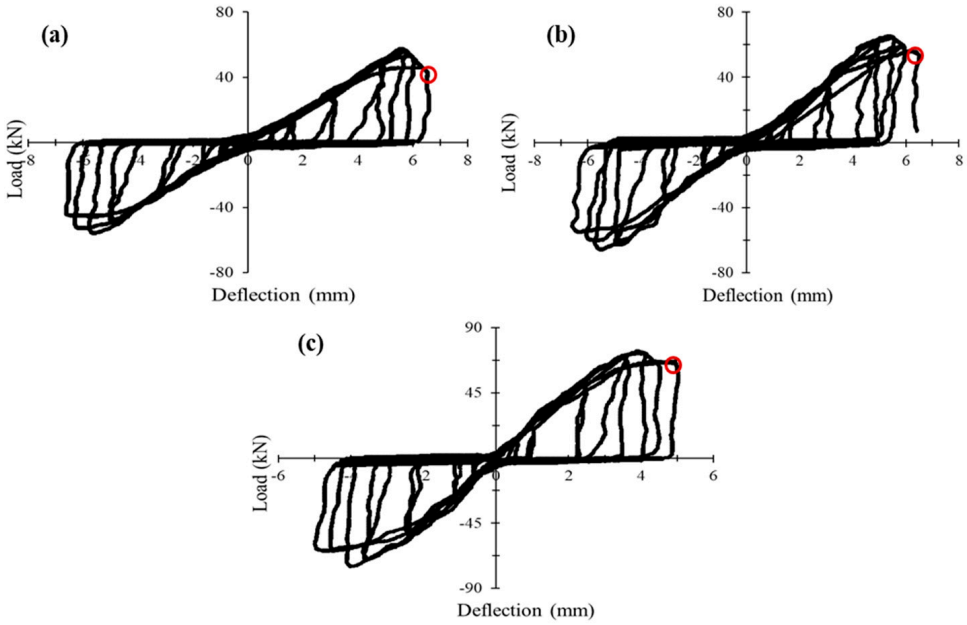


Figure 19. Load–deflection hysteresis curve for ZCC-30 with a/d = 2: (**a**) (2Ø10), (**b**) (3Ø10), (**c**) (3Ø12).

For a shear span-to-depth ratio of a/d = 2.5, the load–deflection hysteresis behavior of ZCC beams is shown in Figures 20 and 21 (the small red circles in the figures indicate the ultimate failure points), with corresponding test data provided in Table 8. Increasing the compressive strength from 20 MPa to 30 MPa resulted in ultimate load increases of 20.34%, 18.59%, and 13.11%, while deflections decreased by approximately 10.82%, 6.83%, and 18.40% for beams reinforced with 2Ø10, 3Ø10, and 3Ø12, respectively. The increase in compressive strength further enhanced stiffness and reduced deformation, improving load performance under cyclic conditions.

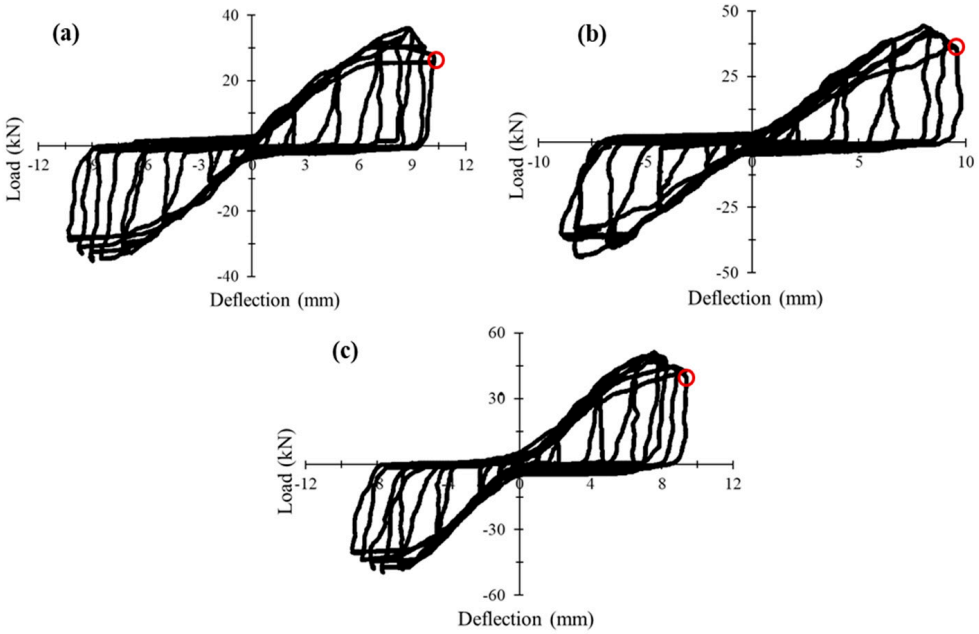


Figure 20. Load–deflection hysteresis curve for ZCC-20 with a/d = 2.5: (**a**) (2Ø10), (**b**) (3Ø10), (**c**) (3Ø12).

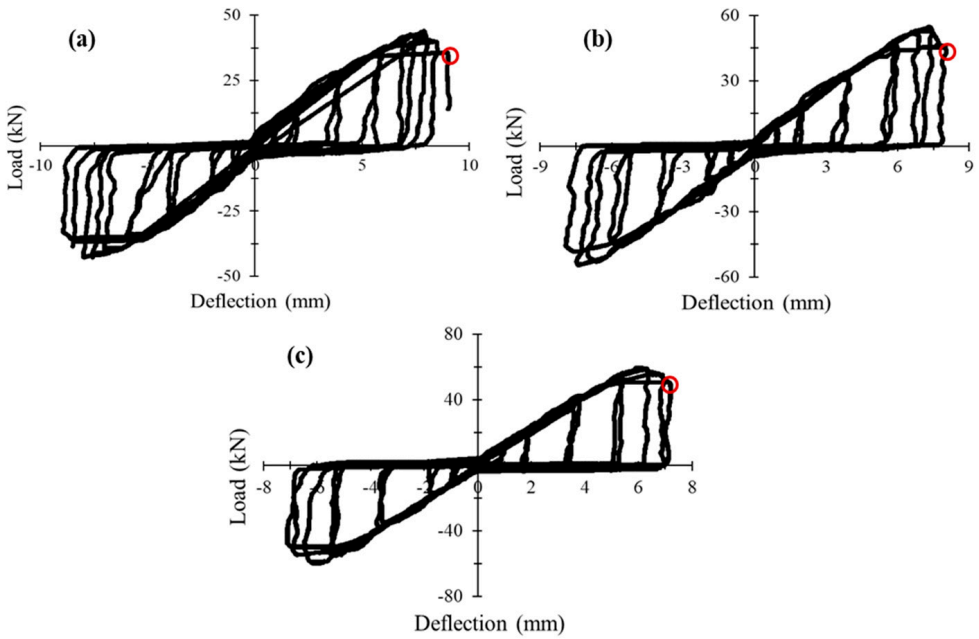


Figure 21. Load–deflection hysteresis curve for ZCC-30 with a/d = 2.5: (**a**) (2Ø10), (**b**) (3Ø10), (**c**) (3Ø12).

Table 8. Experimental results for beams ZCC-20 and ZCC-30 under cyclic loading with a/d = 2.5.

Group	ρ	P_u (kN)	Δ_u (mm)	K (kN/mm)	No. of Cycles to Failure	Energy Absorption (kN.mm)
ZCC-20 (2Ø10)	0.0065	35.25	9.01	3.91	12	2242.98
ZCC-20 (3Ø10)	0.0097	44.15	8.13	5.43	12	2579.72
ZCC-20 (3Ø12)	0.0141	51.35	7.61	6.75	12	2760.04
ZCC-30 (2Ø10)	0.0065	44.25	7.91	5.59	13	2110.91
ZCC-30 (3Ø10)	0.0097	54.23	7.42	7.31	11	2201.15
ZCC-30 (3Ø12)	0.0141	59.1	6.18	9.56	11	2392.12

When the shear span-to-depth ratio increased to a/d = 3, the cyclic response became more flexure-dominated in nature. Figures 22 and 23 (the small red circles in the figures indicate the ultimate failure points) and Table 9 summarize the results for ZCC beams with compressive strengths of 20 MPa and 30 MPa. The ultimate load increased by 13.22%, 13.59%, and 16.80%, while the corresponding deflections decreased by 7.14%, 6.29%, and 6.30% for beams reinforced with 2Ø10, 3Ø10, and 3Ø12 bars, respectively. The enhanced load-carrying capacity at higher compressive strength is attributed to improved material stiffness and a stronger bond interaction between the reinforcement and the geopolymeric binder. The hysteresis loops indicate stable cyclic behavior, with only minor stiffness reduction and delayed crack propagation across successive cycles.

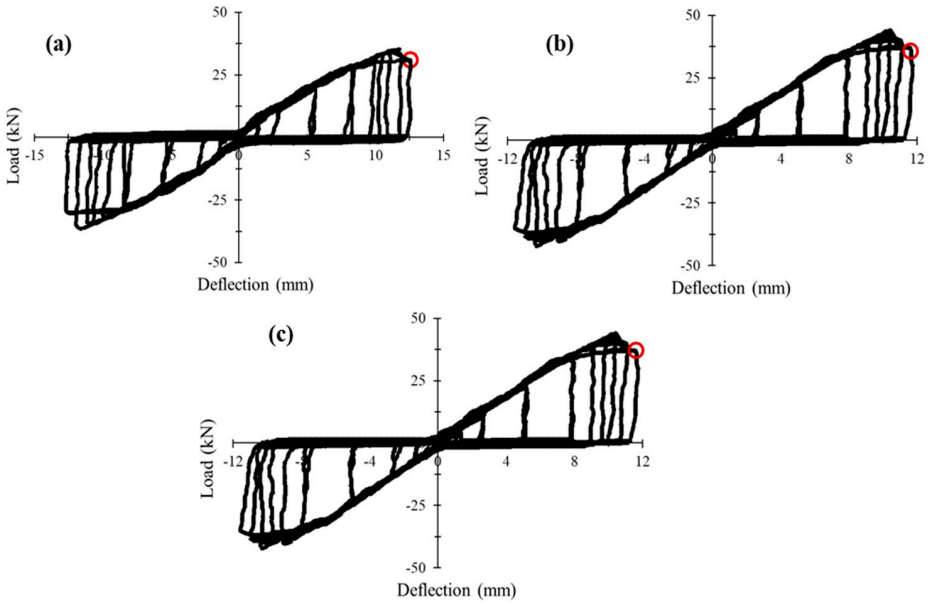


Figure 22. Load–deflection hysteresis curve for ZCC-20 with a/d = 3.0: (**a**) (2Ø10), (**b**) (3Ø10), (**c**) (3Ø12).

Table 9. Experimental results for beams ZCC-20 and ZCC-30 under cyclic loading with a/d = 3.

Group	ρ	P_u (kN)	Δ_u (mm)	K (kN/mm)	No. of Cycles to Failure	Energy Absorption (kN.mm)
ZCC-20 (2Ø10)	0.0065	34.74	11.26	3.09	13	3125.5
ZCC-20 (3Ø10)	0.0097	44.19	10.65	4.15	13	3354.84
ZCC-20 (3Ø12)	0.0141	49.13	9.78	5.02	13	3742.86
ZCC-30 (2Ø10)	0.0065	40.03	10.51	3.81	13	3386.44
ZCC-30 (3Ø10)	0.0097	51.14	10.02	5.10	13	4196.25
ZCC-30 (3Ø12)	0.0141	59.05	9.2	6.42	14	4330.03

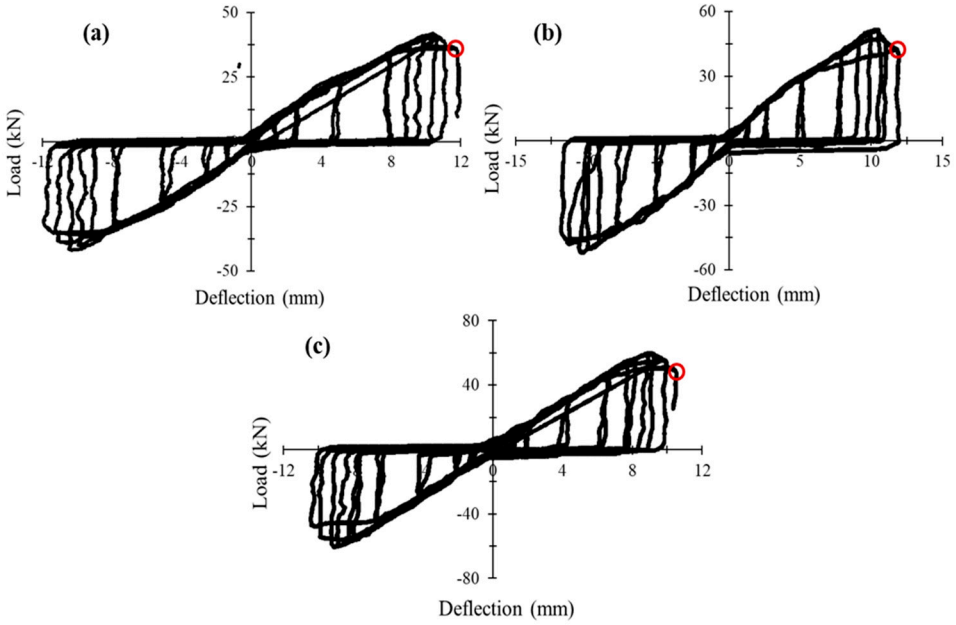


Figure 23. Load–deflection hysteresis curve for ZCC-30 with a/d = 3.0: (**a**) (2Ø10), (**b**) (3Ø10), (**c**) (3Ø12).

The effect of the shear span-to-effective depth ratio (a/d) on the cyclic response is further analyzed in Table 10. Increasing the a/d ratio from 2 to 2.5 caused a reduction in ultimate load by 20.25–33.87%, accompanied by an increase in deflection by 22.20–35.76%. When the ratio increased from 2 to 3, the ultimate load decreased by 27.51–44.09%, while deflection increased by 37.74–56.85%. These trends confirm that increasing a/d reduces the contribution of shear forces, shifting the response from shear-dominated to flexural behavior. Consequently, beams with higher a/d values exhibited larger deflections and lower load capacities but still maintained stable cyclic behavior with considerable energy dissipation, demonstrating the ductile nature of ZCC under repeated loading.

Table 10. Comparative results of shear span-to-depth ratio for ZCC-20 and ZCC-30 beams with a/d = 2, 2.5, and 3; 2Ø10, 3Ø10, 3Ø12 reinforcement.

Group	*a/d*	Difference Ultimate Load %	Difference Ultimate Deflection %
ZCC-20 (2Ø10)	2.5 to 2	−32.91 *	22.20
	3 to 2.5	−1.47	19.98
	3 to 2	−34.86	37.74
ZCC-30 (2Ø10)	2.5 to 2	−30.35	29.58
	3 to 2.5	−10.54	24.74
	3 to 2	−44.09	47.00
ZCC-20 (3Ø10)	2.5 to 2	−27.88	24.85
	3 to 2.5	0.09	23.66
	3 to 2	−27.77	42.63
ZCC-30 (3Ø10)	2.5 to 2	−20.25	26.42
	3 to 2.5	−6.04	25.95
	3 to 2	−27.51	45.51
ZCC-20 (3Ø12)	2.5 to 2	−33.87	26.02
	3 to 2.5	−4.52	22.19
	3 to 2	−39.91	42.43
ZCC-30 (3Ø12)	2.5 to 2	−27.55	35.76
	3 to 2.5	−0.08	32.83
	3 to 2	−27.65	56.85

* The minus signs indicate a decrease in the ultimate load.

3.3. Effect of Reinforcement Ratio and Compressive Strength

Although different longitudinal bar configurations were adopted in the experimental program, their structural effects are discussed herein primarily in terms of the corresponding longitudinal reinforcement ratio (ρ). The bar arrangements are retained only for specimen identification.

The influence of reinforcement ratio and compressive strength on the load–deflection response of ZCC beams was investigated for a/d ratios of 2, 2.5, and 3. The main longitudinal reinforcement consisted of steel bars with diameters Ø10 and Ø12, arranged as 2Ø10, 3Ø10, or 3Ø12, corresponding to ρ values of 0.0065, 0.0097, and 0.0141, respectively. The comparative results for different reinforcement configurations and compressive strengths (20 and 30 MPa) are presented in Tables 11 and 12 for monotonic and cyclic loading, respectively, while the corresponding load–deflection relationships for monotonic loading are shown in Figure 24.

Table 11. Comparative results of steel reinforcement for ZCC-20 and ZCC-30 beams with a/d = 2, 2.5, and 3 under monotonic loading.

Group	*a/d*	Steel Bar Comparison	Difference Ultimate Load %	Difference Ultimate Deflection %
ZCC-20	2	3Ø10 to 2Ø10	14.11	−11.83 *
		3Ø12 to 3Ø10	17.65	−5.84
		3Ø12 to 2Ø10	29.27	−18.36
ZCC-30	2	3Ø10 to 2Ø10	12.93	−5.22
		3Ø12 to 3Ø10	14.29	−16.16
		3Ø12 to 2Ø10	25.37	−22.22
ZCC-20	2.5	3Ø10 to 2Ø10	19.48	−8.77
		3Ø12 to 3Ø10	16.74	−6.88
		3Ø12 to 2Ø10	32.96	−16.25
ZCC-30	2.5	3Ø10 to 2Ø10	17.87	−6.53
		3Ø12 to 3Ø10	13.41	−12.21
		3Ø12 to 2Ø10	28.88	−19.54
ZCC-20	3	3Ø10 to 2Ø10	18.56	−8.18
		3Ø12 to 3Ø10	16.37	−3.46
		3Ø12 to 2Ø10	31.89	−11.92
ZCC-30	3	3Ø10 to 2Ø10	16.63	−2.12
		3Ø12 to 3Ø10	14.84	−15.16
		3Ø12 to 2Ø10	29.00	−17.60

* The minus signs indicate a decrease in the ultimate deflection.

Table 12. Comparative results of steel bar configurations for ZCC-20 and ZCC-30 beams with a/d = 2, 2.5, and 3 under cyclic loading.

Group	*a/d*	Steel Bar Comparison	Difference Ultimate Load %	Difference Ultimate Deflection %
ZCC-20	2	3Ø10 to 2Ø10	17.02	−14.73 *
		3Ø12 to 3Ø10	13.42	−11.90
		3Ø12 to 2Ø10	8.81	−41.81
ZCC-30	2	3Ø10 to 2Ø10	17.02	−14.73
		3Ø12 to 3Ø10	17.86	−8.53
		3Ø12 to 2Ø10	31.84	−40.30
ZCC-20	2.5	3Ø10 to 2Ø10	20.16	−10.82
		3Ø12 to 3Ø10	14.02	−6.83
		3Ø12 to 2Ø10	31.35	−18.40

Table 12. *Cont.*

Group	*a*/*d*	Steel Bar Comparison	Difference Ultimate Load %	Difference Ultimate Deflection %
ZCC-30	2.5	3Ø10 to 2Ø10	18.40	−6.60
		3Ø12 to 3Ø10	8.24	−20.06
		3Ø12 to 2Ø10	25.13	−27.99
ZCC-20	3	3Ø10 to 2Ø10	21.38	−5.73
		3Ø12 to 3Ø10	10.05	−15.13
		3Ø12 to 2Ø10	29.29	−15.13
ZCC-30	3	3Ø10 to 2Ø10	21.72	−4.89
		3Ø12 to 3Ø10	13.40	−8.91
		3Ø12 to 2Ø10	32.21	−14.24

* The minus signs indicate a decrease in the ultimate deflection.

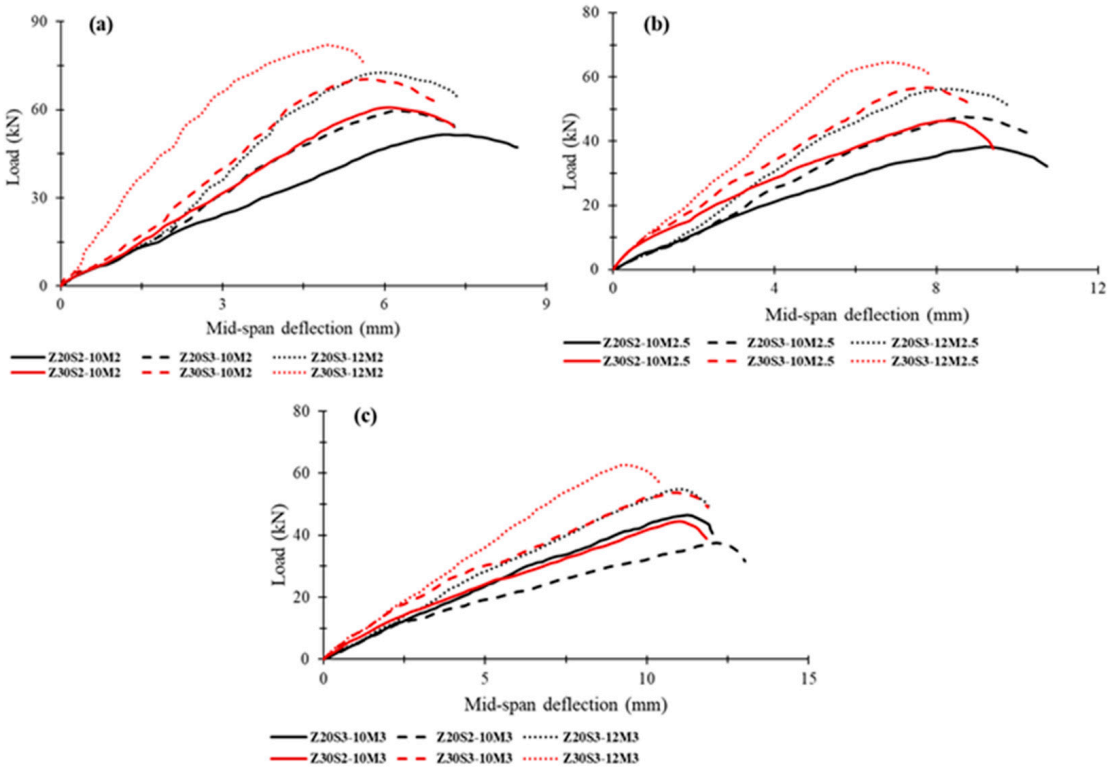


Figure 24. Mid-span load–deflection curves for ZCC beams with f'_c = 20 and 30 MPa, reinforcement ratios (2Ø10, 3Ø10, 3Ø12), and shear span-to-depth ratios of (**a**) a/d = 2, (**b**) a/d = 2.5, (**c**) a/d = 3.0 (Note: **Z20S2-10M2** indicates f'_c = 20, 2Ø10 steel, and a/d = 2.0 and so on).

It is evident that increasing the longitudinal reinforcement ratio enhances the beam's load-carrying capacity and slightly reduces deflection. For beams with compressive strengths of 20 and 30 MPa, the increase in the longitudinal reinforcement ratio (ρ), corresponding to the transition from 2Ø10 to 3Ø10, resulted in an average improvement in ultimate load of approximately 14–17%, while increasing from 3Ø10 to 3Ø12 led to a further 13–18% increase. Correspondingly, ultimate deflection decreased by 5–15%, indicating improved stiffness and crack control. This improvement is attributed to the greater tensile resistance and enhanced dowel action of the additional steel, which facilitates more efficient shear transfer through aggregate interlock and reduces crack widths. The increase in bar number (from two to three) proved more effective than increasing bar diameter, as it provides a larger total surface area for stress transfer and improves confinement of the surrounding concrete.

Table 11 indicates that beams with a higher reinforcement ratio demonstrated greater ductility before failure, particularly under shear-dominated conditions (a/d = 2), where

the combined action of steel dowel resistance and the dense geopolymer matrix helped delay crack propagation and mitigate premature failure. At larger a/d ratios (2.5 and 3), where flexural behavior dominated, the influence of reinforcement on load capacity remained significant but had a more limited effect on deflection reduction, as deformation was primarily governed by flexural curvature.

A detailed comparison in Table 12 confirms that increasing the longitudinal reinforcement ratio (ρ), corresponding to the reinforcement ratio by approximately 33% (from 2Ø10 to 3Ø10) and 31% (from 3Ø10 to 3Ø12), improved ultimate load by up to 32% while decreasing deflection by up to 28%, depending on strength level and a/d ratio. Beams with f'_c = 30 MPa consistently carried higher loads and exhibited smaller deflections than those with 20 MPa, highlighting the combined contribution of compressive strength and reinforcement in enhancing structural stiffness and energy absorption. Figure 24 clearly demonstrates that increasing both f'_c and ρ leads to steeper load–deflection curves and greater post-yield ductility, confirming the synergistic effect of material strength and reinforcement content in improving flexural performance.

Consequently, the results confirm that the structural efficiency of ZCC beams can be substantially enhanced through increased reinforcement ratio and concrete compressive strength. The higher steel ratio not only augments the beam's load capacity through improved tensile resistance and dowel action but also stabilizes post-cracking behavior, resulting in greater energy absorption and delayed failure. These trends demonstrate that ZCC, when properly reinforced, exhibits a ductile and reliable response comparable to that of NC under both shear and flexural loadings.

3.4. Cracking Patterns and Shear Failure Modes

The formation and propagation of cracks provide essential insight into the mechanisms governing beam failure under shear and flexural stresses. In the tested beams, the most prominent cracks were consistently observed near the supports, where diagonal shear cracks developed and propagated from the beam's tension zone at the bottom toward the compression zone at the top surface. These inclined cracks are characteristic of shear-dominated behavior and were predominantly observed in specimens with a/d between 2 and 2.5. The inclination of these cracks generally ranged between 30° and 45° relative to the horizontal axis, consistent with classical shear failure behavior. Severe spalling and localized crushing of concrete were evident in these regions, indicating a predominantly brittle shear failure mode dominated by diagonal tension.

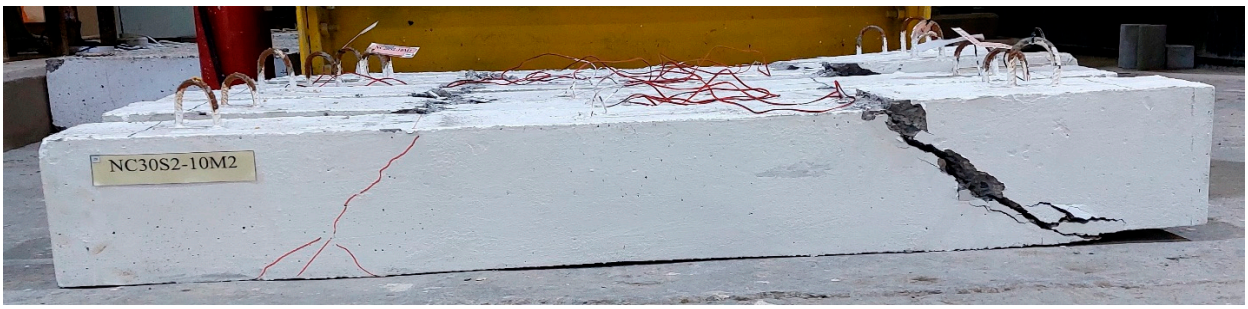
Except for the NC-20 (2Ø10) and NC-30 (2Ø10) specimens, most beams failed in a similar region near the supports and exhibited comparable diagonal shear crack patterns. This behavior is attributed to the consistent shear span-to-depth ratios and reinforcement layouts governing stress concentration and crack propagation. The NC beams with lower reinforcement ratios showed earlier crack localization due to reduced dowel action and weaker bond performance. In contrast, ZCC beams exhibited more uniform crack distribution and stable diagonal shear failure, which is associated with the denser geopolymeric matrix and improved steel-concrete bond.

For specimens tested with a higher shear span-to-depth ratio (a/d = 3), the observed cracking behavior was notably different. The cracks initiated primarily in the central lower region (tension zone) and extended vertically upward, occasionally forming short flexural cracks in the upper compression zone. These cracks were finer and less inclined than those in lower a/d specimens, indicating that the dominant behavior had shifted from shear to flexure. The distribution and shape of these cracks suggest that flexural stresses were more pronounced before the onset of any major shear distress.

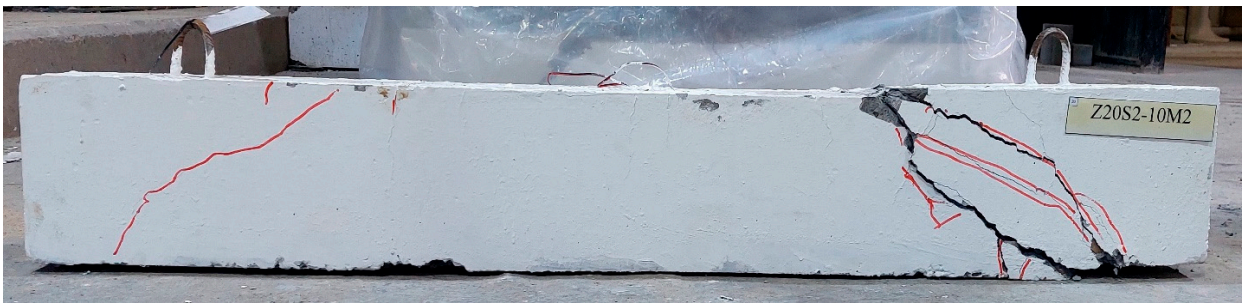
The representative crack patterns for both NC and ZCC beams with compressive strengths of f'_c = 20 MPa and 30 MPa, reinforced with 2Ø10, 3Ø10, and 3Ø12 steel bars under monotonic and cyclic loading, are presented in Figures 25 and 26. Due to their extensive graphical content, the complete sets of crack pattern illustrations for all test configurations are provided in Appendix A, while Figures 25 and 26 present selected examples to demonstrate the typical behavior. Cracks were marked at peak load during testing, while photographs were taken after unloading for documentation purposes. These figures clearly illustrate the transition from shear-dominated cracking at lower shear span-to-depth ratios (a/d = 2) to flexure-dominated behavior as a/d increases to 2.5 and 3.



(**a**) NC-20 (2Ø10) a/d = 2



(**b**) NC-30 (2Ø10) a/d = 2

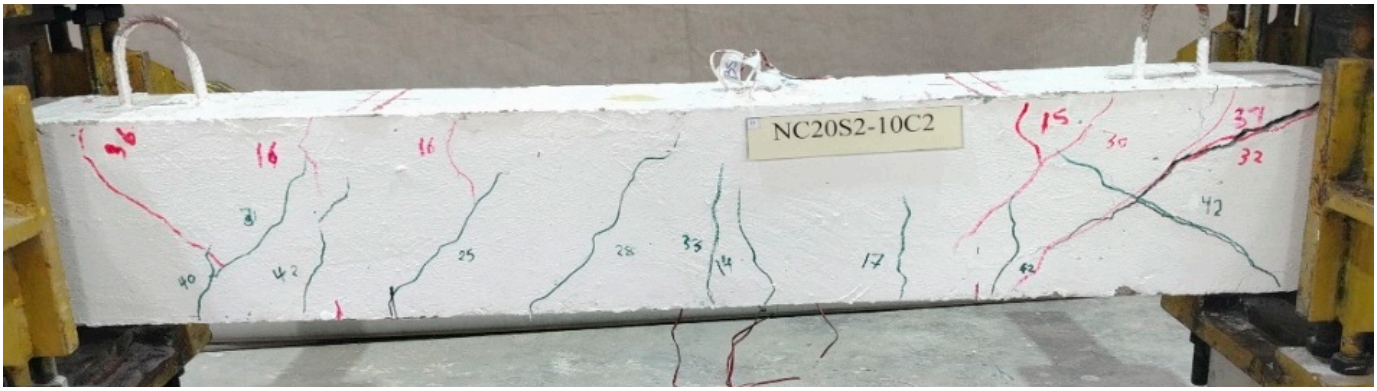


(**c**) ZCC-20 (2Ø10) a/d = 2



(**d**) ZCC-30 (2Ø10) a/d = 2

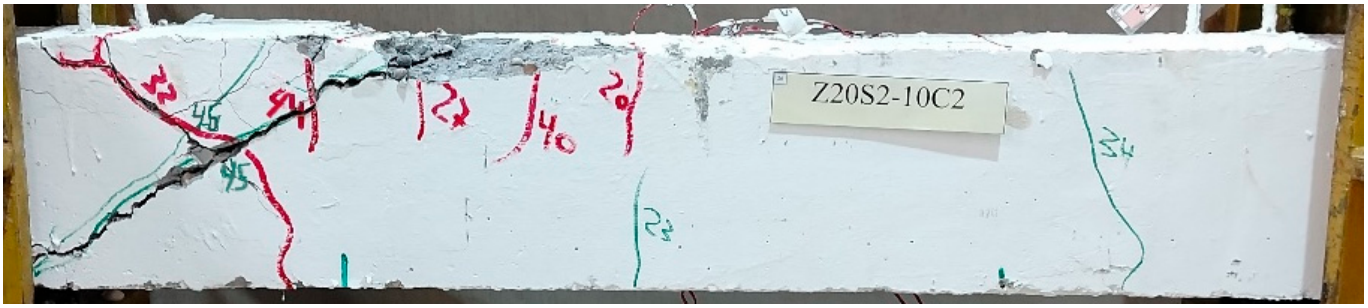
Figure 25. Crack pattern of ZCC beams identified at peak load under monotonic loading (documented during testing; photographed after unloading for clarity) (complete cracking patterns are provided in Appendix A).



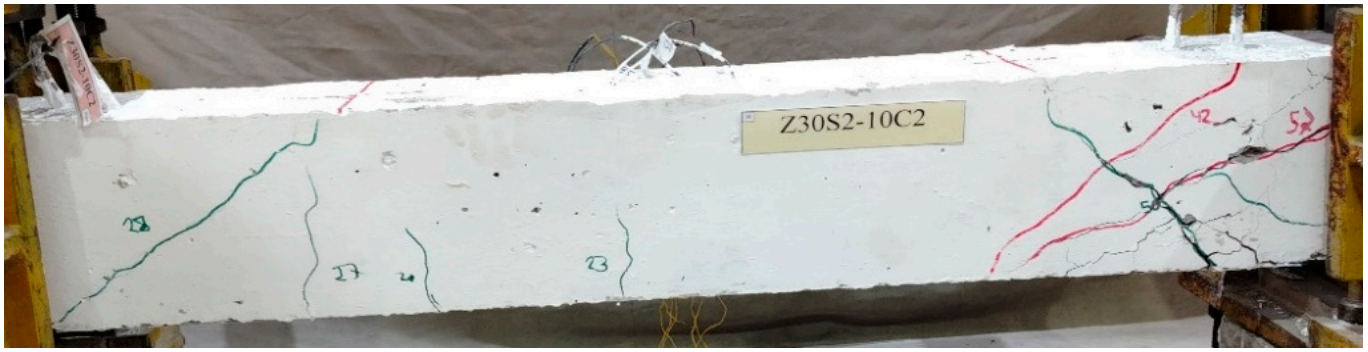
(**a**) NC-20 (2Ø10) $a/d = 2$



(**b**) NC-30 (2Ø10) $a/d = 2$



(**c**) ZCC-20 (2Ø10) $a/d = 2$



(**d**) ZCC-30 (2Ø10) $a/d = 2$

Figure 26. Crack pattern of ZCC beams identified at peak load under cyclic loading (cracks mapped during testing; photographs taken after unloading for clarity) (complete cracking patterns are provided in Appendix A).

3.5. Discussion

For clarity, the influence of longitudinal reinforcement is interpreted based on the reinforcement ratio (ρ), rather than individual bar configurations, to allow consistent comparison among specimens. The experimental results obtained in this study demonstrate that the shear behavior of ZCC beams under both monotonic and cyclic loading is comparable to or exceeds that of conventional NC beams. The observed diagonal shear cracking patterns and failure locations are consistent with those reported by Yacob et al. [17] and Wan et al. [12], who noted similar shear failure mechanisms in fly ash-based geopolymer beams with comparable shear span-to-depth ratios. Critically, however, the present work extends those studies in two important respects.

First, regarding shear capacity: Wan et al. [12] reported $V_{u,exp}/V_{u,ACI}$ ratios of approximately 1.15–1.30 for one-part geopolymer beams. The present study yields average ratios of 1.39 at a/d = 2.0, demonstrating that fly ash-based ZCC systems can achieve even greater shear reserve strength relative to code predictions, particularly at moderate compressive strengths (20–30 MPa). Al-Jabali et al. [6] reported ambient-cured alkali-activated beams achieving shear capacities within 5–8% of OPC counterparts. The present ZCC beams surpassed NC beams by 5.5–10.1% in ultimate shear load at 20 MPa and by 6.8–10.1% at 30 MPa, indicating superior performance across both strength levels.

Second, regarding cyclic performance: Jothivel and Basil Ahamed [22] reported cumulative energy absorption approximately 10–20% higher for geopolymer beams than for OPC beams. The present study demonstrates energy absorption improvements of 5–48% over NC under cyclic loading, with the wider range attributable to the combined influence of reinforcement ratio and compressive strength, parameters not simultaneously varied in prior studies. Furthermore, ZCC beams in the present study sustained 70–90% of their monotonic displacement capacity under cyclic loading, compared to the 60–75% retention reported by Yacob et al. [17] for similar geopolymer systems with lower reinforcement ratios. This improvement highlights the role of both the dense geopolymeric matrix and the higher reinforcement ratios adopted herein in delaying stiffness degradation and enhancing fatigue tolerance.

To assess the applicability of conventional design models, the experimentally measured shear capacities of ZCC beams under monotonic loading were compared with predictions from ACI 318-19 [25] as reported in Tables 3–5. The results indicate that the ACI model provides conservative estimates of shear strength for ZCC beams, with experimental-to-predicted shear strength ratios exceeding unity for all tested specimens except the (a/d = 3.0) case. This suggests that existing OPC-based shear design provisions can be safely applied to ZCC beams for preliminary design, although material-specific calibration may further enhance accuracy.

The increase in shear capacity with higher compressive strength and reinforcement ratio observed in this study aligns with findings reported by Al-Jabali et al. [6] and Özkılıç et al. [15], who attributed improved load resistance to enhanced matrix density and improved steel–concrete bonding in geopolymer systems. Furthermore, the reduction in load capacity and increase in deflection with increasing a/d ratio are consistent with classical reinforced concrete behavior and previous experimental observations on geopolymer beams [17,23].

Under cyclic loading, ZCC beams exhibited stable hysteresis loops, slower stiffness degradation, and higher cumulative energy absorption compared to NC beams, which is in agreement with earlier studies by Jothivel and Basil Ahamed [22] and Al-Janabi et al. [14]. These findings confirm that geopolymer binders can effectively sustain repeated loading through improved crack control and stress redistribution mechanisms. Load transfer between concrete and reinforcement is governed by bond stress, dowel action,

aggregate interlock, and compression strut action. After diagonal cracking, shear resistance is dominated by dowel action and aggregate interlock. The dense geopolymeric matrix in ZCC enhances bond quality and crack-bridging capacity, resulting in more stable load transfer and reduced degradation under cyclic loading.

Based on the experimental results, optimal shear performance of ZCC beams was achieved at higher compressive strength (30 MPa), increased longitudinal reinforcement ratio, and lower shear span-to-depth ratio (a/d = 2). These parameters resulted in higher load capacity, improved stiffness, and enhanced energy dissipation under both monotonic and cyclic loading. The observed trends provide a practical experimental basis for identifying optimal design ranges and can serve as reference data for future analytical or numerical modeling studies.

It should be noted that the compressive strength levels investigated in this study (20 and 30 MPa) fall within the normal-to-moderate strength range as defined by ACI 318-19 [25] and EN 206:2013+A2:2021 [26], which classify these values within the standard strength classes (C16/20 and C25/30, respectively) typically adopted for reinforced beams, slabs, and other shear-critical structural members in low- to mid-rise construction. While higher-strength concretes are increasingly used in specialized applications, the selected strength range reflects common practice and allows meaningful assessment of shear behavior and crack development, which are often more critical at moderate strength levels. Nevertheless, the authors acknowledge that the performance of zero-cement concrete at higher strength grades was not addressed in this study. Further experimental investigations are therefore required to evaluate the shear and cyclic response of high-strength geopolymer concrete beams and to support broader structural adoption.

Overall, the close agreement between the present results and those reported in the literature confirms the reliability of the experimental program and demonstrates that ZCC beams can achieve shear performance and cyclic resilience comparable to, or exceeding, that of conventional concrete beams.

4. Conclusions

This study evaluated the shear behavior of reinforced ZCC beams under monotonic and cyclic loading, focusing on the effects of concrete compressive strength, reinforcement ratio, and shear span-to-effective depth ratio. Based on the findings of the experimental program, the following conclusions can be drawn.

- ZCC beams exhibited cracking and failure patterns similar to those of NC beams, characterized by diagonal shear cracks inclined at 30–45°.
- Increasing compressive strength from 20 to 30 MPa enhanced load capacity by 12–17% and reduced deflection by 5–21%.
- For zero-cement concrete (ZCC) beams, increasing the longitudinal reinforcement ratio (ρ = 0.0065–0.014) enhanced the load-carrying capacity by approximately 13–33% and slightly reduced deflection due to increased stiffness and improved crack control. In addition, higher reinforcement ratios increased energy absorption by about 5–15%, indicating improved ductility and deformation capacity under shear-dominated behavior.
- Varying the shear span ratio (a/d = 2–3) reduced ultimate load by 2–37% and increased deflection by 24–48%, indicating a shift toward flexural behavior.
- ZCC beams maintained stable hysteresis loops and deformation capacity similar to that of NC beams. Ultimate loads were increased by 2–14%, while deflection was increased by 2–17%.

- Increasing compressive strength from 20 to 30 MPa improved load capacity by up to 20% and reduced deflection by 4–21%.
- Under cyclic loading, ZCC beams with higher reinforcement ratios (ρ = 0.0065–0.0141) exhibited enhanced load-carrying capacity by approximately 8–32%, accompanied by reduced deflection and a substantial increase in energy absorption (5–48%). The formation of diagonal and X-shaped cracks under load reversals confirms a ductile shear-dominated response with effective stress redistribution and improved cyclic resilience.
- Under cyclic loading, increasing the shear span-to-depth ratio (a/d = 2–3) reduced ultimate load capacity by 20–44% and increased deflection by 20–57%, reflecting a clear transition from shear-dominated to flexure-dominated response and greater susceptibility to fatigue-induced degradation.

ZCC beams exhibited stiffness, load capacity, and cyclic performance comparable to or exceeding those of OPC beams. Under cyclic loading, ZCC achieved 2–14% higher ultimate load capacity, 2–17% greater deformation capacity, and 5–48% higher energy absorption, indicating enhanced ductility and fatigue resistance. These improvements are attributed to the dense geopolymeric matrix, which improves steel–concrete bond behavior, delays crack propagation, and reduces stiffness degradation. Accordingly, ZCC can be considered a practical and eco-efficient alternative to OPC for shear-dominated structural elements.

This study is limited to longitudinal reinforcement and specific geopolymer compositions; the effects of transverse shear reinforcement, curing regimes, durability, environmental exposure, and analytical or numerical modeling were not addressed. Future work should investigate these parameters, including large-scale and seismic loading, and develop validated analytical and numerical models for predicting the shear response of ZCC beams. In addition, although not addressed herein, previous studies indicate that ZCC can significantly reduce CO_2 emissions relative to OPC, warranting future life-cycle cost and environmental impact assessments.

Author Contributions: M.A.Q.A.-J.: Conceptualization, Methodology, Supervision, Investigation, Visualization, Writing—review and editing. D.A.-J.: Methodology, Software, Data curation, Formal analysis, Writing—original draft, Writing—review and editing. R.T.N.: Methodology, Investigation, Data curation. L.F.A.B.: Visualization, Writing—review and editing. I.B.M.J.: Writing—review and editing. H.A.S.P.: Writing—review and editing. All authors have read and agreed to the published version of the manuscript.

Funding: This work was partially supported by the GeoBioTec Research Unit, through the strategic projects UIDB/04035/2025 (https://doi.org/10.54499/UIDB/04035/2025) and UIDP/04035/2020 (https://doi.org/10.54499/UIDP/04035/2025), funded by the Fundação para a Ciência e a Tecnologia, IP/MCTES through national funds (PIDDAC). Funding for the period 2025–2029-transition phase.

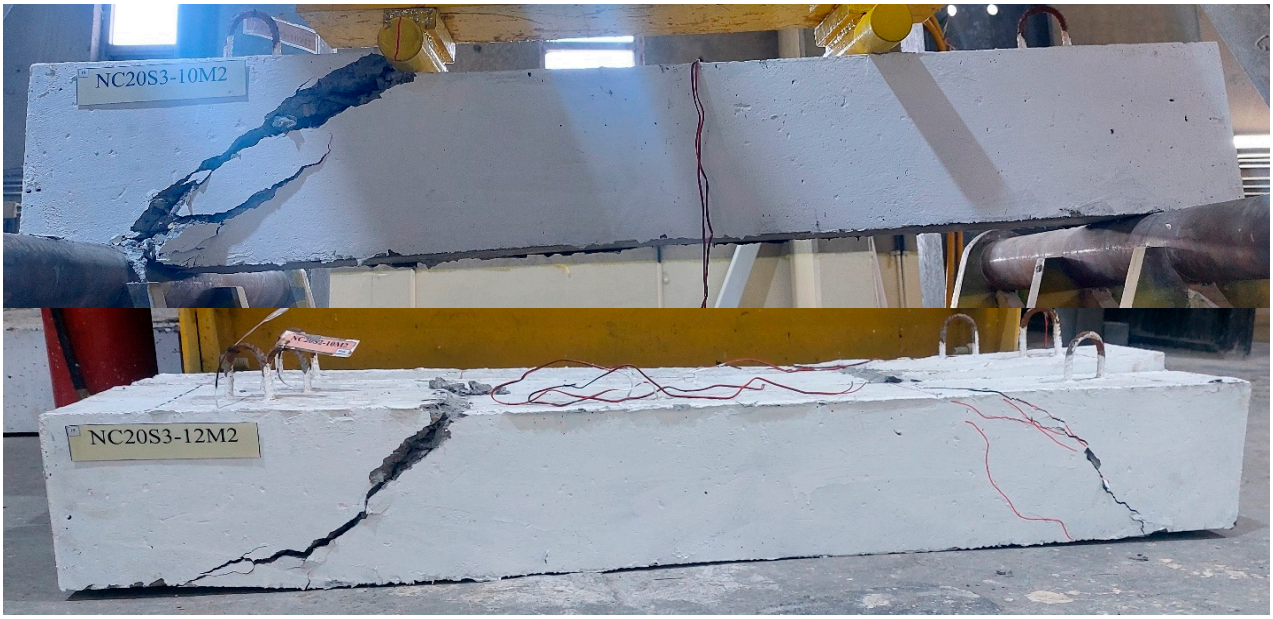
Institutional Review Board Statement: Not applicable.

Informed Consent Statement: Not applicable.

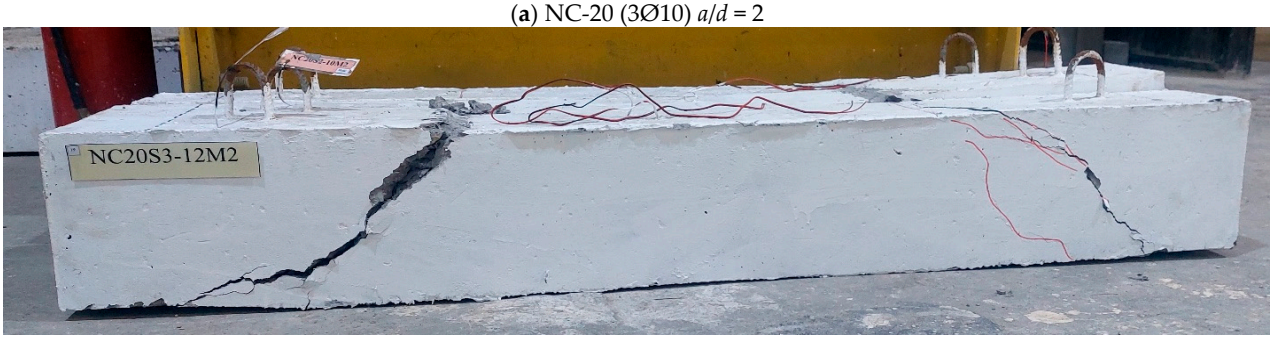
Data Availability Statement: The authors declare that the data supporting the findings of this study are available within the paper.

Conflicts of Interest: The authors declare no conflicts of interest.

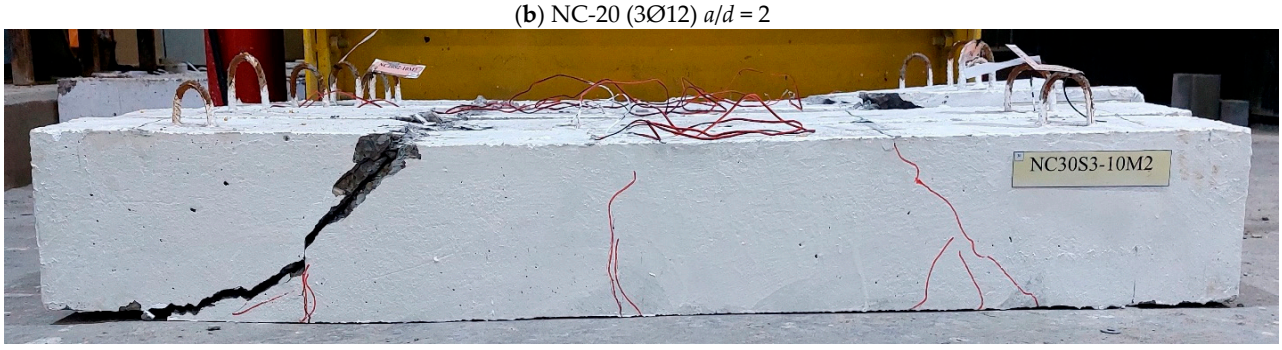
Appendix A



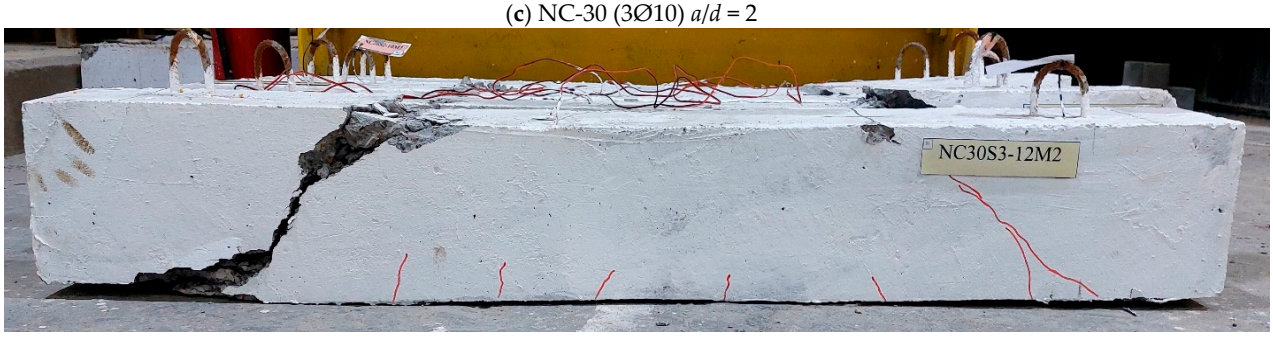
(**a**) NC-20 (3Ø10) $a/d = 2$



(**b**) NC-20 (3Ø12) $a/d = 2$

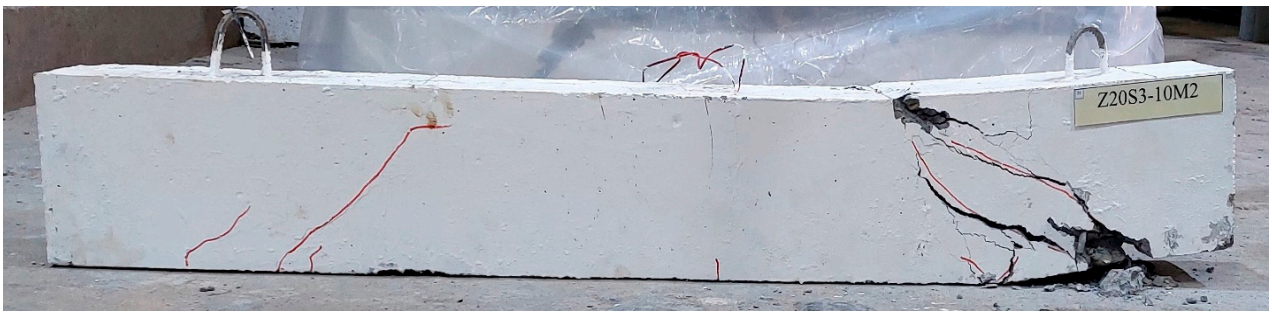


(**c**) NC-30 (3Ø10) $a/d = 2$

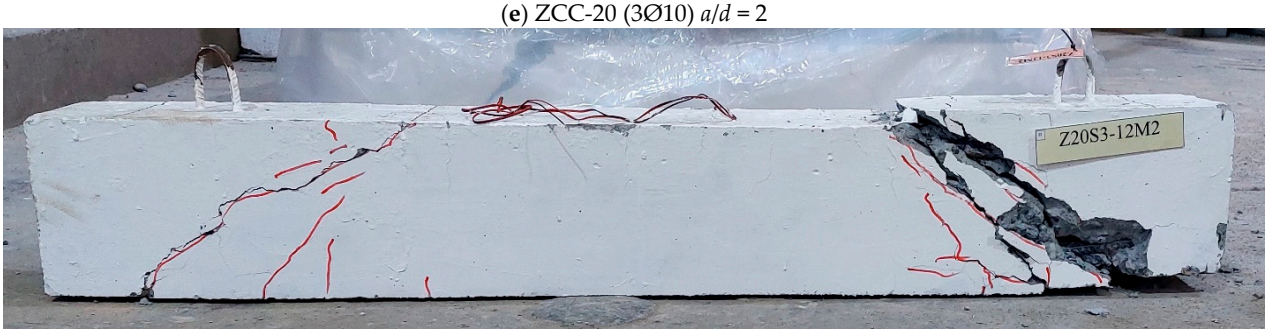


(**d**) NC-30 (3Ø12) $a/d = 2$

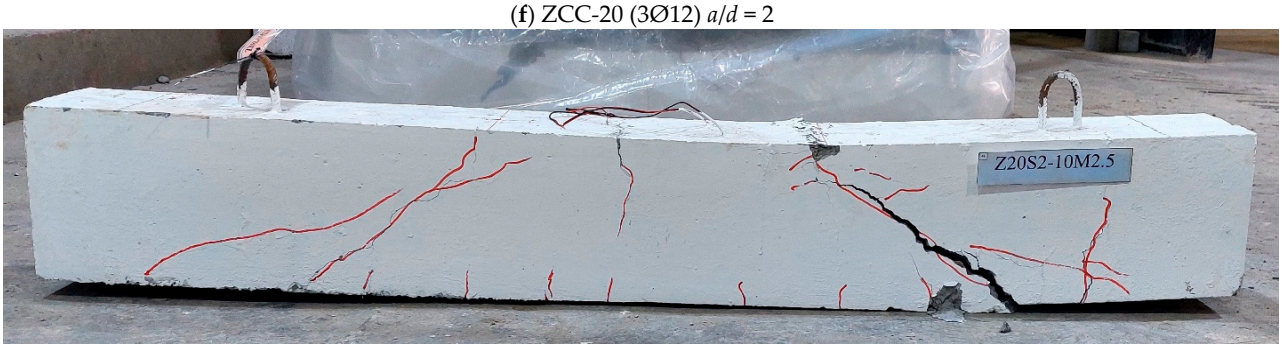
Figure A1. *Cont.*



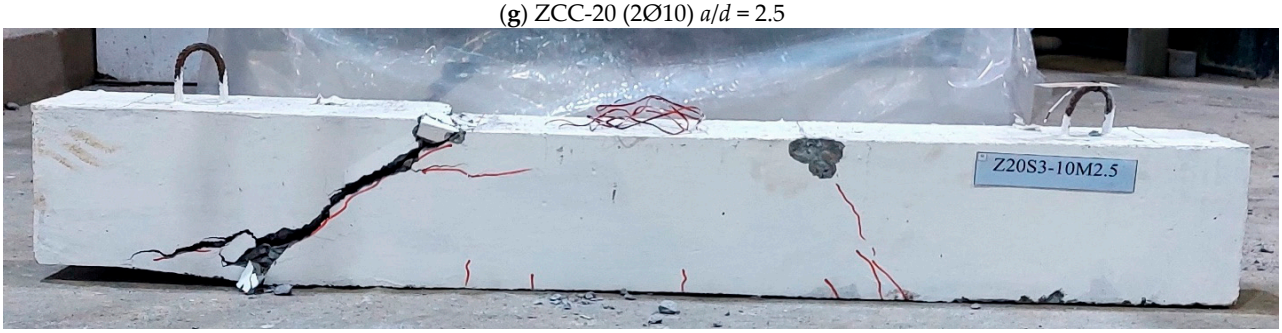
(**e**) ZCC-20 (3Ø10) a/d = 2



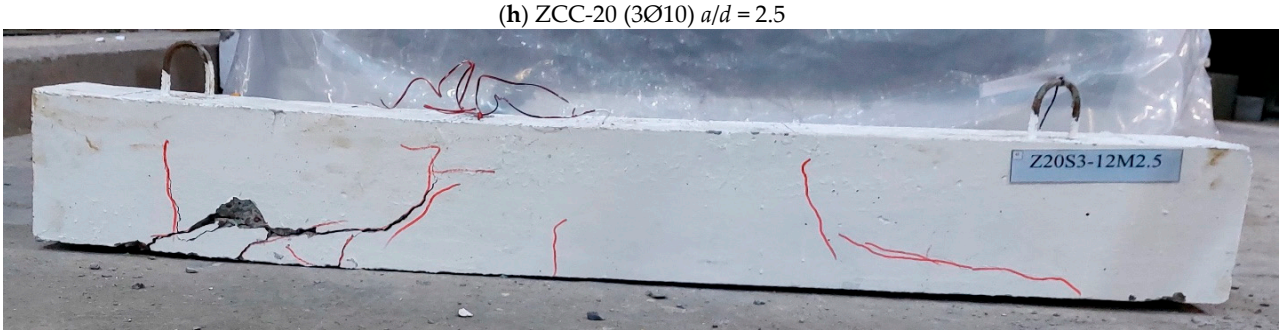
(**f**) ZCC-20 (3Ø12) a/d = 2



(**g**) ZCC-20 (2Ø10) a/d = 2.5

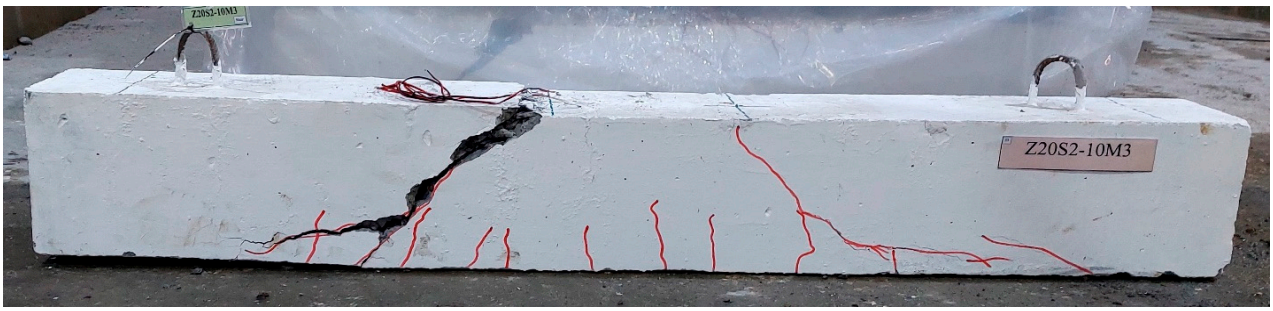


(**h**) ZCC-20 (3Ø10) a/d = 2.5

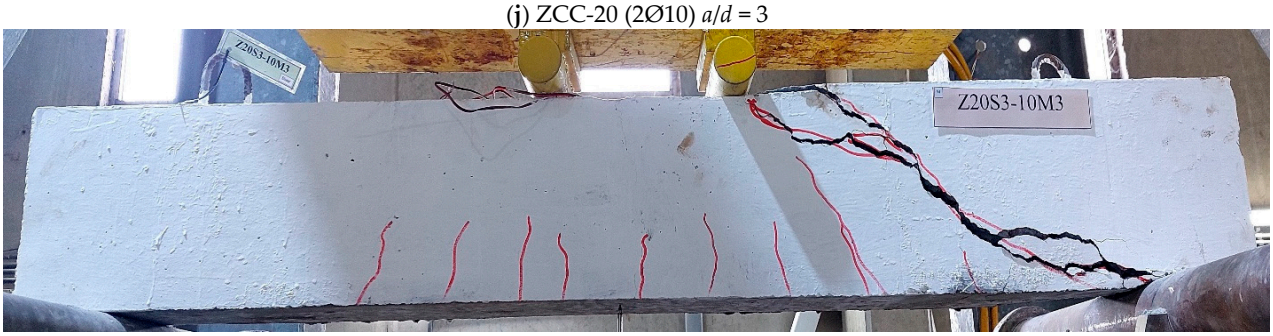


(**i**) ZCC-20 (3Ø12) a/d = 2.5

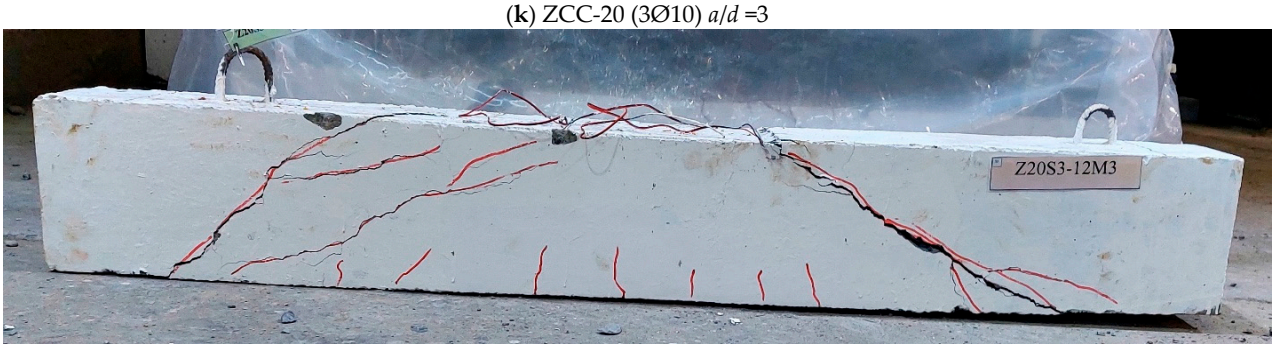
Figure A1. *Cont.*



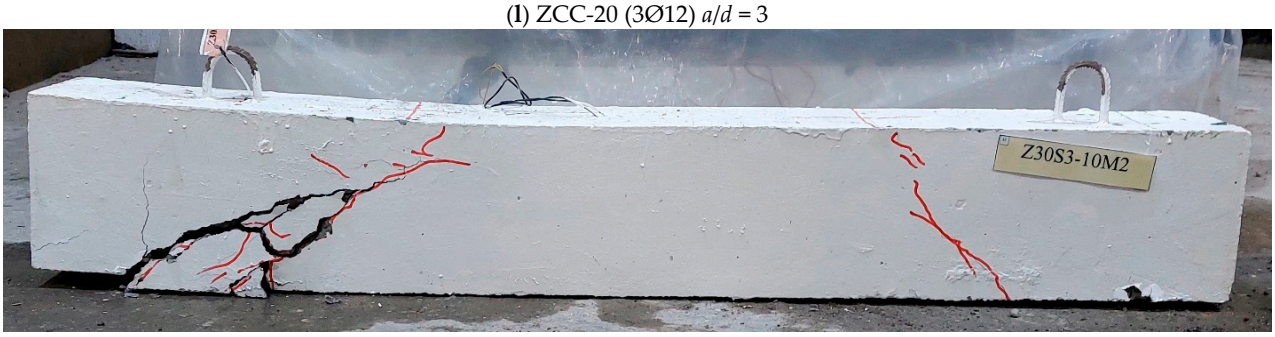
(**j**) ZCC-20 (2Ø10) a/d = 3



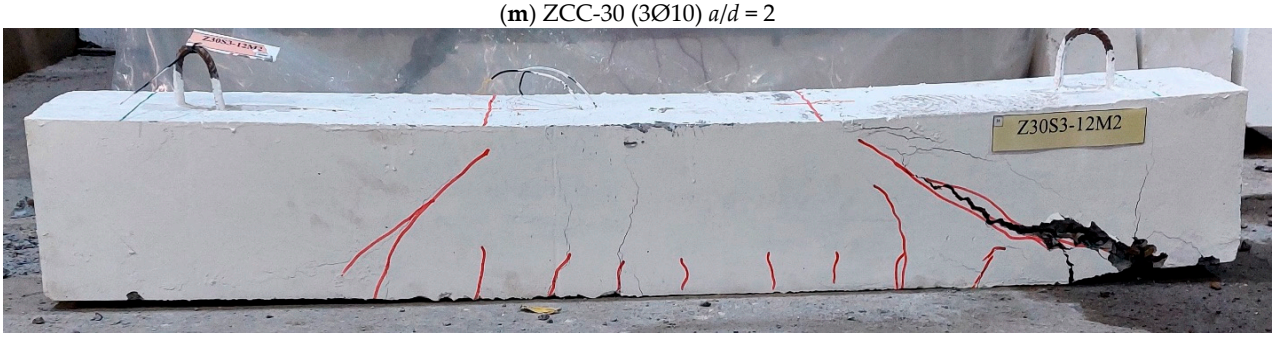
(**k**) ZCC-20 (3Ø10) a/d =3



(**l**) ZCC-20 (3Ø12) a/d = 3

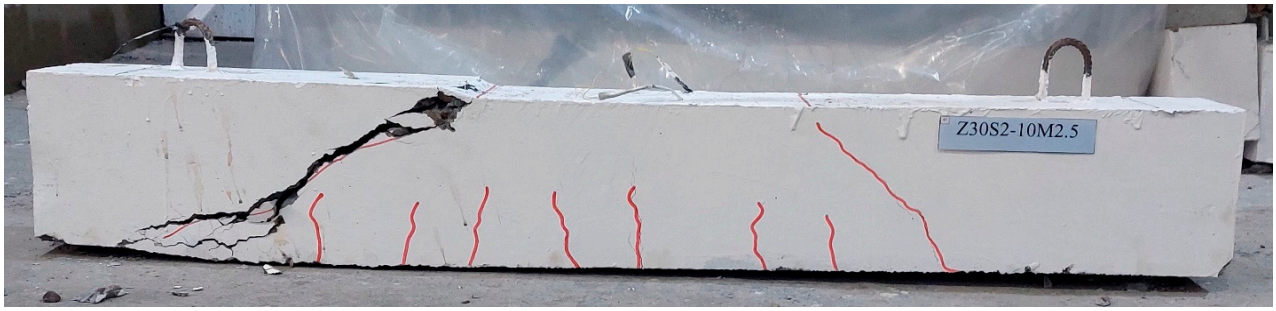


(**m**) ZCC-30 (3Ø10) a/d = 2

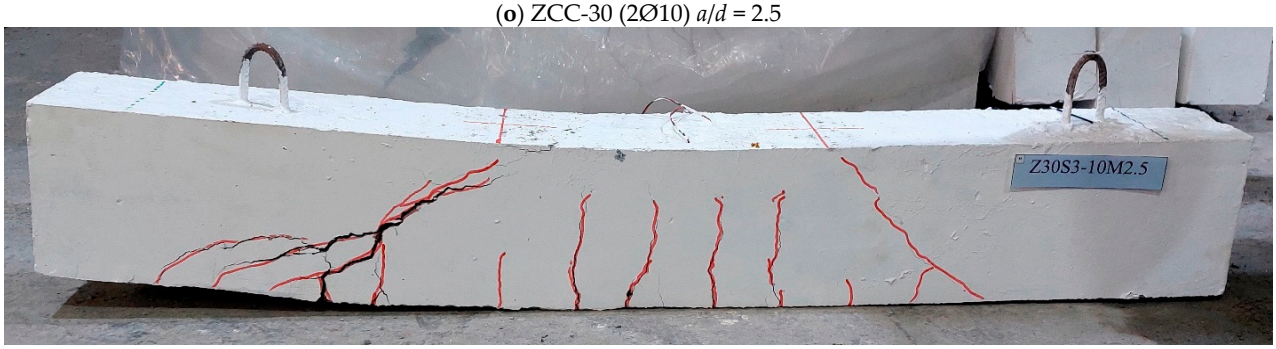


(**n**) ZCC-30 (3Ø12) a/d = 2

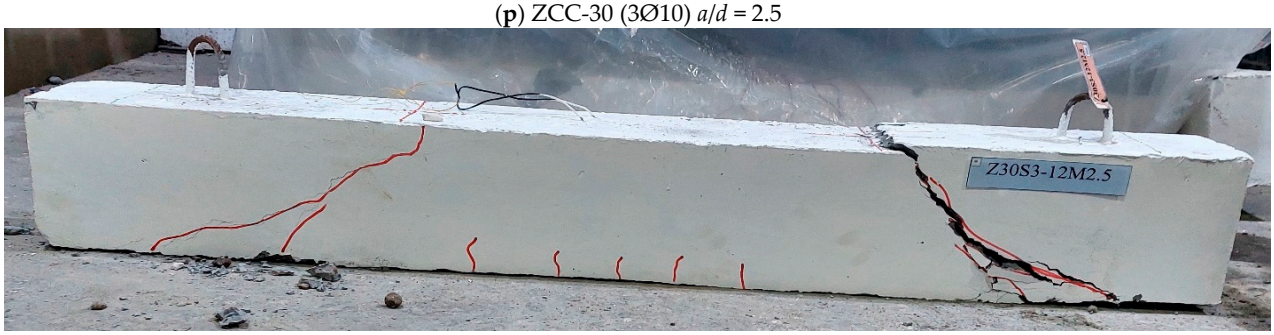
Figure A1. *Cont.*



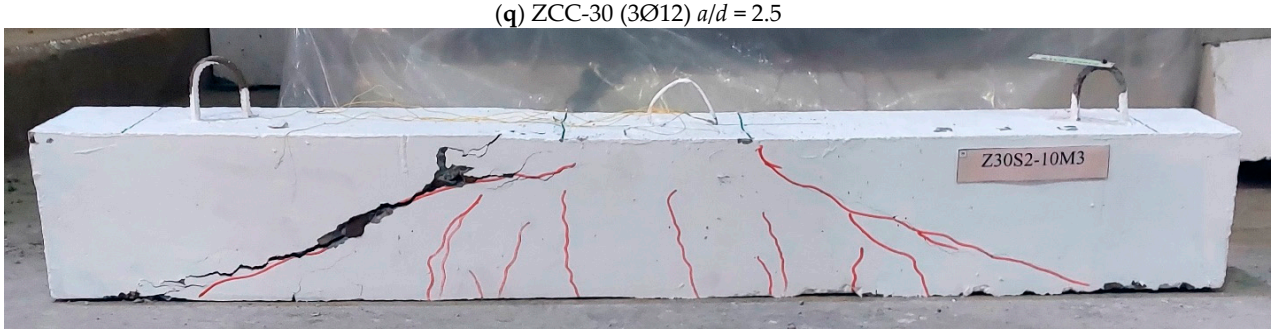
(**o**) ZCC-30 (2Ø10) *a*/*d* = 2.5



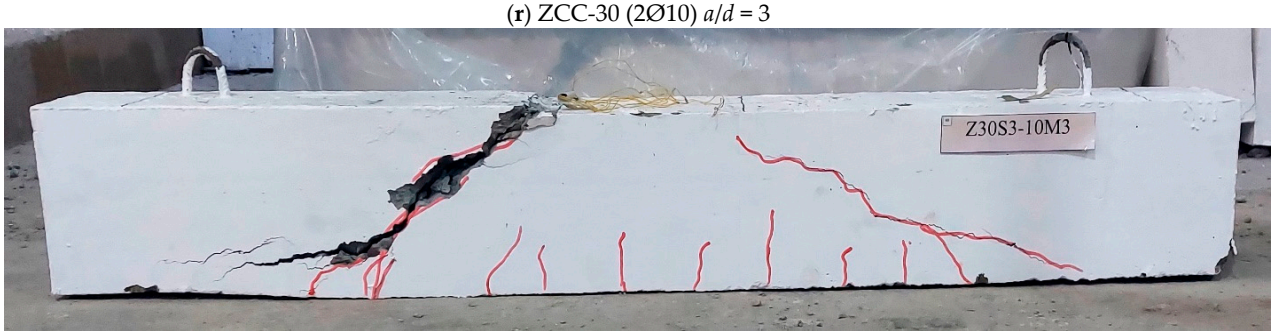
(**p**) ZCC-30 (3Ø10) *a*/*d* = 2.5



(**q**) ZCC-30 (3Ø12) *a*/*d* = 2.5



(**r**) ZCC-30 (2Ø10) *a*/*d* = 3



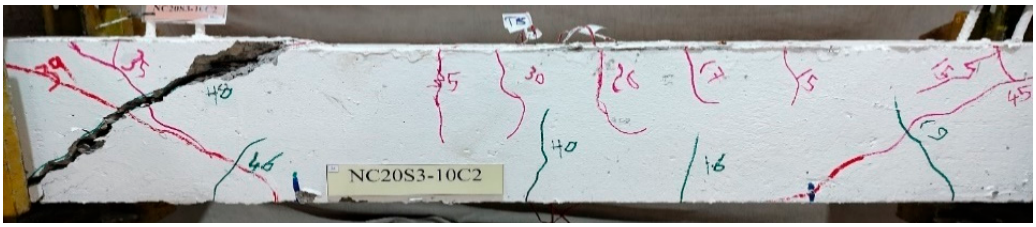
(**s**) ZCC-30 (3Ø10) *a*/*d* = 3

Figure A1. *Cont.*

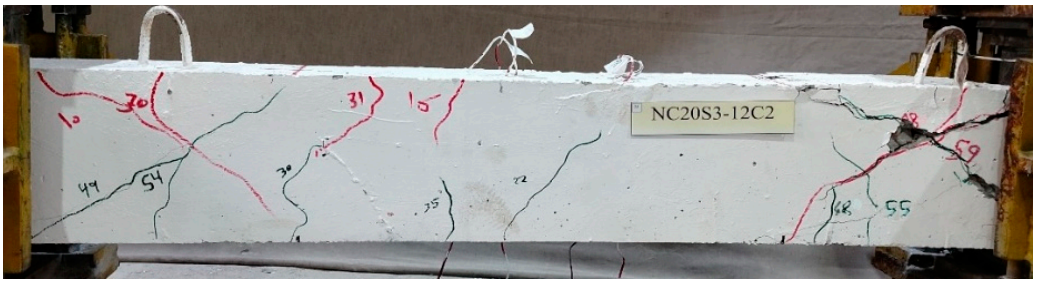


(**t**) ZCC-30 (3Ø12) a/d = 3

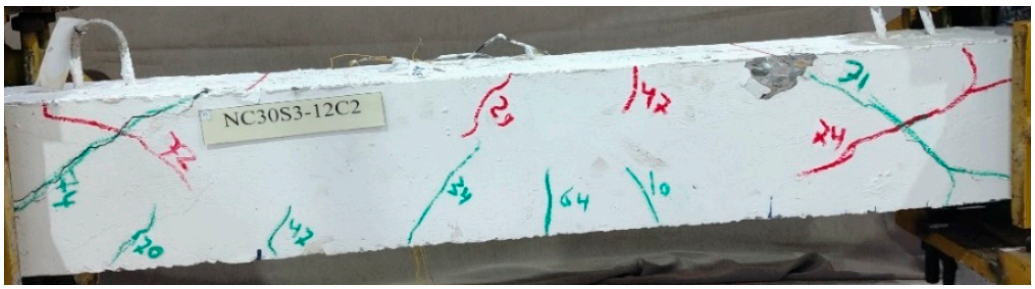
Figure A1. Complete crack patterns of ZCC-20 and ZCC-30 beams under monotonic loading with different reinforcement ratios (2Ø10, 3Ø10, and 3Ø12) and shear span-to-depth ratios (a/d = 2, 2.5, and 3).



(**a**) NC-20 (3Ø10) a/d = 2



(**b**) NC-20 (3Ø12) a/d = 2

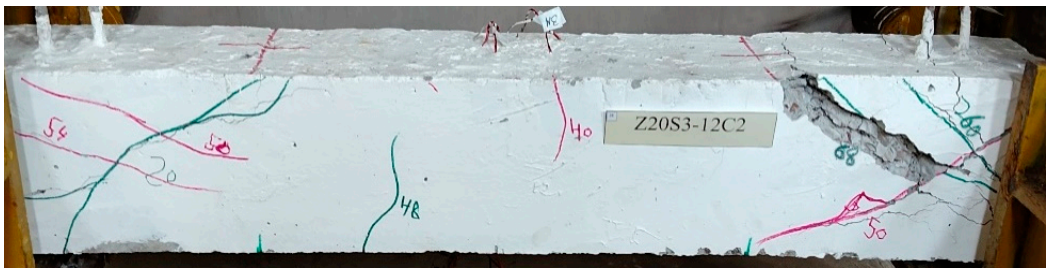


(**c**) NC-30 (3Ø12) a/d = 2

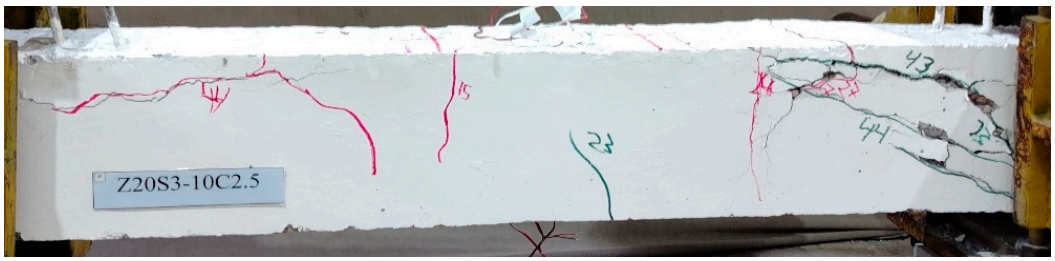


(**d**) ZCC-20 (3Ø10) a/d = 2

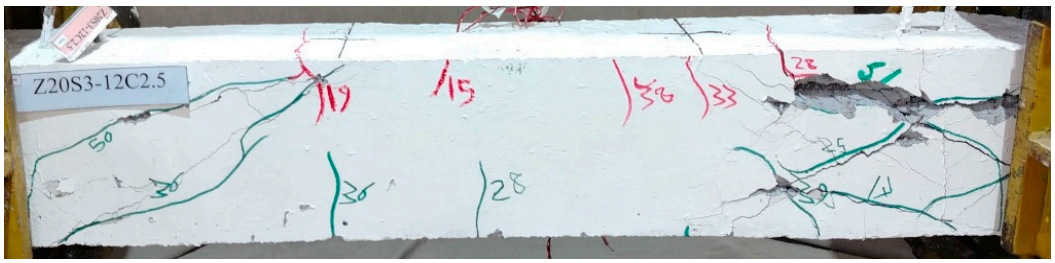
Figure A2. *Cont.*



(**e**) ZCC-20 (3Ø12) a/d = 2



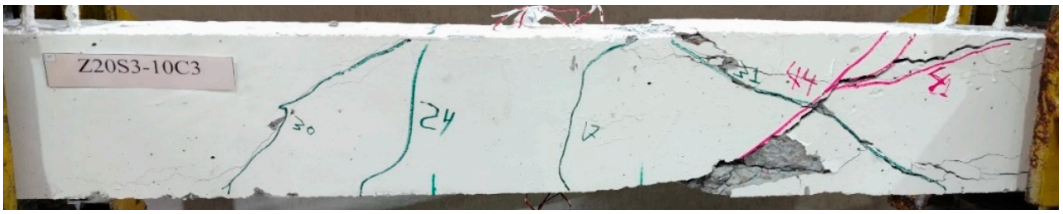
(**f**) ZCC-20 (3Ø10) a/d = 2.5



(**g**) ZCC-20 (3Ø12) a/d = 2.5



(**h**) ZCC-20 (2Ø10) a/d = 3



(**i**) ZCC-20 (3Ø10) a/d = 3



(**j**) ZCC-20 (3Ø12) a/d = 3

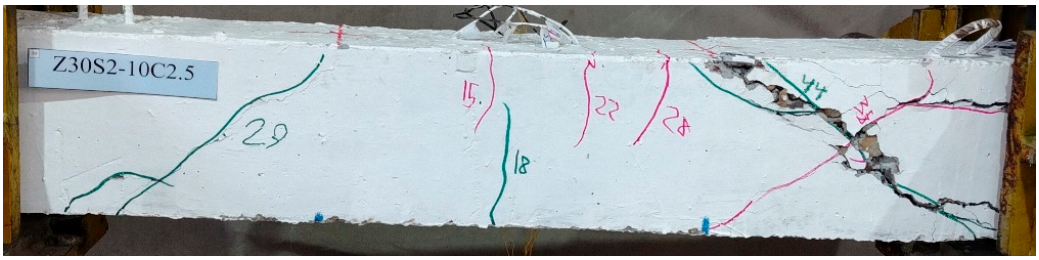
Figure A2. *Cont.*



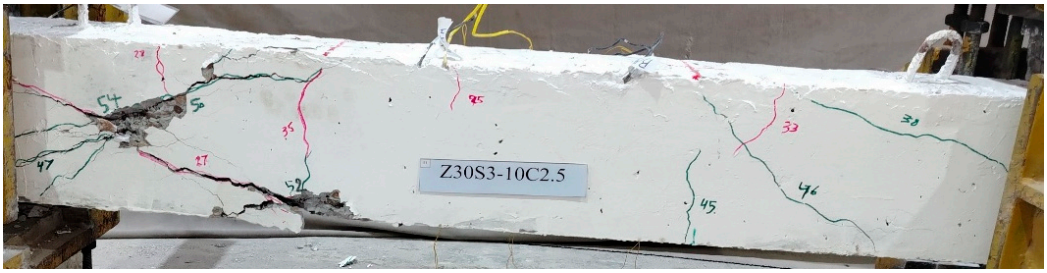
(**k**) ZCC-30 (3Ø10) a/d = 2



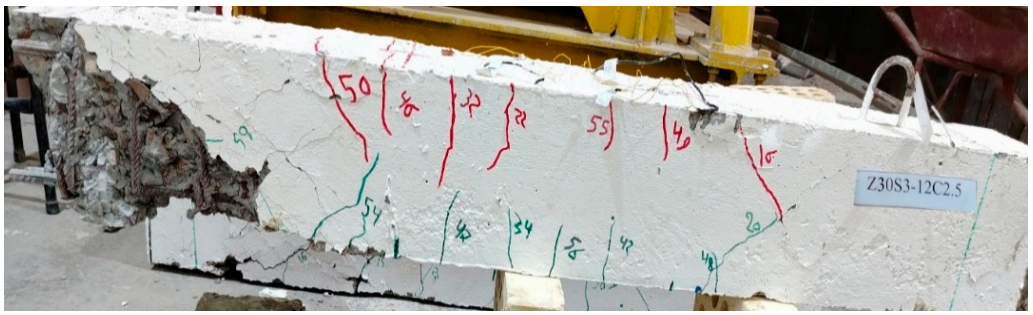
(**l**) ZCC-30 (3Ø12) a/d = 2



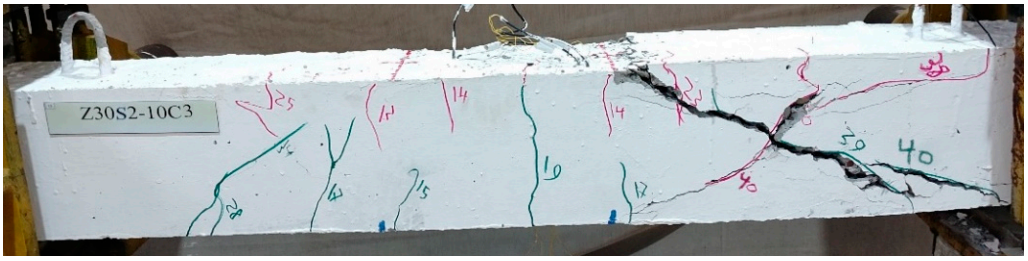
(**m**) ZCC-30 (2Ø10) a/d = 2.5



(**n**) ZCC-30 (3Ø10) a/d = 2.5

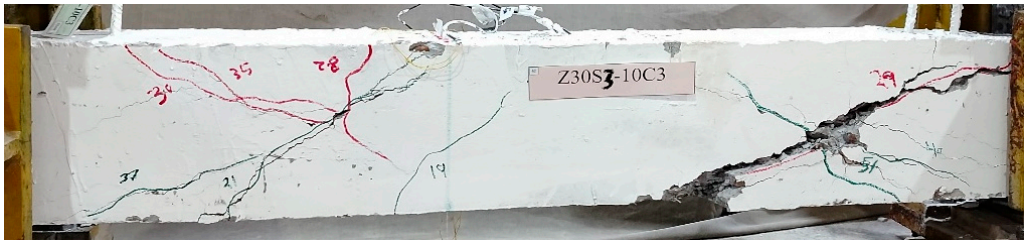


(**o**) ZCC-30 (3Ø12) a/d = 2.5



(**p**) ZCC-30 (2Ø10) a/d = 3

Figure A2. *Cont.*



(**q**) ZCC-30 (3Ø10) a/d = 3



(**r**) ZCC-30 (3Ø12) a/d = 3

Figure A2. Complete crack patterns of ZCC-20 and ZCC-30 beams under cyclic loading with different reinforcement ratios (2Ø10, 3Ø10, and 3Ø12) and shear span-to-depth ratios (a/d = 2, 2.5, and 3).

References

1. Cao, Z.; Masanet, E.; Tiwari, A.; Akolawala, S. *Decarbonizing Concrete: Deep Decarbonization Pathways for the Cement and Concrete Cycle in the United States, India, and China*; Industrial Sustainability Analysis Laboratory, Northwestern University: Evanston, IL, USA, 2021.
2. Amran, M.; Debbarma, S.; Ozbakkaloglu, T. Fly ash-based eco-friendly geopolymer concrete: A critical review of the long-term durability properties. *Constr. Build. Mater.* **2020**, *270*, 121857. [CrossRef]
3. Provis, J.L.; Bernal, S.A. Geopolymers and related alkali-activated materials. *Annu. Rev. Mater. Res.* **2014**, *44*, 299–327. [CrossRef]
4. Davidovits, J. Properties of Geopolymer Cements. In *First International Conference on Alkaline Cements and Concretes*; Kiev State Technical University: Kiev, Ukraine, 1994; pp. 131–149.
5. Wallah, S.E.; Rangan, B.V. *Low-Calcium Fly Ash-Based Geopolymer Concrete: Long Term Properties*; Research Report GC 2; Faculty of Engineering, Curtin University of Technology: Perth, Australia, 2006.
6. Al-Jabali, H.M.; El-Latief, A.A.; Ezz, M.S.; Khairy, S.; Nada, A.A. GGBFS and Red-Mud Based Alkali-Activated Concrete Beams: Flexural, Shear and Pull-Out Test Behavior. *Civ. Eng. J.* **2024**, *10*, 123–145. [CrossRef]
7. Kumar, B.S.C.; Ramesh, K. Analytical study on flexural behaviour of reinforced geopolymer concrete beams by ANSYS. *Mater. Sci. Eng.* **2018**, *455*, 012065.
8. Sinaei, H.; Shariati, M.; Abna, A.H.; Aghaei, M.; Shariati, A. Evaluation of reinforced concrete beam behavior using finite element analysis by ABAQUS. *Sci. Res. Essays* **2012**, *7*, 2002–2009.
9. Hassoon, M.M.; Qissab, M.A. Performance of Zero Cement Concrete Synthesized from Fly Ash: A Critical Review. *E3S Web Conf.* **2023**, *437*, 04002. [CrossRef]
10. Hassoon, M.M.; Al-Janabi, M.A.Q. Behavior of Zero Cement Reinforced Concrete Slabs under Monotonic and Impact Loads: Experimental and Numerical Investigations. *Case Stud. Constr. Mater.* **2024**, *21*, e03789. [CrossRef]
11. Hassoon, M.M.; Qissab, M.A. Behavior of Reinforced Zero Cement Concrete Slabs under Monotonic Load. *Al-Nahrain J. Eng. Sci.* **2024**, *27*, 328–338. [CrossRef]
12. Wan, S.; Zong, Z.; Lin, Y.; Shi, H.; Yuan, Y.; Ding, B.; Cai, J. Shear Behavior of Reinforced One-Part Geopolymer Concrete Beams. *J. Build. Eng.* **2025**, *111*, 113205. [CrossRef]
13. Kannan, H.; Veerappan, S.K.; Sivasubramanian, M.V.R. Experimental and Numerical Investigation of Shear Performance of RC Deep Beams Strengthened with Engineered Cementitious Composites. *Constr. Mater.* **2025**, *5*, 51. [CrossRef]
14. Al-Janabi, M.A.Q.; Al-Jeznawi, D.; Nasser, R.T.; Bernardo, L.F.A.; Pinto, H.A.S. Flexural Performance of Geopolymer-Reinforced Concrete Beams under Monotonic and Cyclic Loading: Experimental Investigation. *Buildings* **2026**, *16*, 209. [CrossRef]
15. Özkılıç, Y.O.; Çelik, A.I.; Aksoylu, C.; Karalar, M.; Mydin, A.O.; Althaqafi, E.; Yılmaz, F.; Umiye, O.A. Shear and flexural performance of reinforced geopolymer concrete beams cured under ambient and oven conditions with environmentally friendly waste steel tire wire additives. *Sci. Rep.* **2025**, *15*, 22765. [CrossRef] [PubMed]
16. Ding, L.; Chen, J.; Caspeele, R. Dynamic sensitive failure mode in the progressive collapse of RC structures subjected to column removal scenarios. *Eng. Struct.* **2025**, *323*, 119301. [CrossRef]

17. Yacob, N.S.; ElGawady, M.A.; Sneeda, L.H.; Said, A. Shear strength of fly ash-based geopolymer reinforced concrete beams. *Eng. Struct.* **2019**, *196*, 109298. [CrossRef]
18. Akduman, S.; Aktepe, R.; Aldemir, A.; Ozcelikci, E.; Yildirim, G.; Sahmaran, M.; Ashour, A. Structural performance of construction and demolition waste-based geopolymer concrete columns under combined axial and lateral cyclic loading. *Eng. Struct.* **2023**, *297*, 116973. [CrossRef]
19. Srinivas, M.R.; Himath Kumar, Y.; Kumar, B.S.C. Studies on flexural behavior of geopolymer concrete beams with GGBS. *Int. J. Recent Technol. Eng.* **2019**, *7*, 105–110.
20. Nagajothi, S.; Elavenil, S.; Angalaeswari, S.; Natrayan, L.; Paramasivam, P. Cracking Behaviour of Alkali-Activated Aluminosilicate Beams Reinforced with Glass and Basalt Fibre-Reinforced Polymer Bars under Cyclic Load. *Int. J. Polym. Sci.* **2022**, *2022*, 6762449. [CrossRef]
21. Tauqir, M.; Qazi, A.U.; Khan, Q.S.; Munir, M.J.; Kazmi, S.M.S. Shear behavior of geopolymer concrete slender beams. *Buildings* **2023**, *13*, 1191. [CrossRef]
22. Jothivel, S.; Basil Ahamed, S. Flexural behaviour of geopolymer concrete beams under cyclic loading. *J. Emerg. Technol. Innov. Res. (JETIR)* **2021**, *8*, 2349–5162.
23. Suraneni, P.; Burris, L.; Shearer, C.R.; Hooton, R.D. ASTM C618 Fly Ash Specification: Comparison with Other Specifications, Shortcomings, and Solutions. *ACI Mater. J.* **2021**, *118*, 157–167. [CrossRef]
24. *ASTM C618*; Standard Specification for Coal Fly Ash and Raw or Calcined Natural Pozzolan for Use in Concrete. ASTM International: West Conshohocken, PA, USA, 2023.
25. *ACI 318-19*; Building Code Requirements for Structural Concrete and Commentary. American Concrete Institute: Farmington Hills, MI, USA, 2019.
26. *EN 206:2013+A2:2021*; Concrete: Specification, Performance, Production and Conformity. CEN: Brussels, Belgium, 2021.

Disclaimer/Publisher's Note: The statements, opinions and data contained in all publications are solely those of the individual author(s) and contributor(s) and not of MDPI and/or the editor(s). MDPI and/or the editor(s) disclaim responsibility for any injury to people or property resulting from any ideas, methods, instructions or products referred to in the content.